Journal of Progressive Medical Sciences
ISSN: 3052-8518
J.P.M.S
https://doi.org/10.63939/1px6w815

Copyright © The Author(s)
Vol. 2 , No. 6 , August 2026

RESEARCH Open Access

Molecular Docking and Phylogenetic Characterization of the *AdeB* Efflux Pump in Clinical Multidrug-Resistant *Acinetobacter baumannii* isolates

Hawraa Natiq Kabroot AL-Fatlawy*

Medical Microbiology, College of Medicine, University of Kufa, Najaf, IRAQ.

hawraan.alfatlawy@uokufa.edu.iq , hawraanatiq@gmail.com , https://orcid.org/0000-0003-0293-8759

Abstract

Background: *Acinetobacter baumannii* has emerged as a major multidrug-resistant pathogen in hospital settings, largely driven by efflux-mediated resistance mechanisms. **Aim and objectives:** This study integrated phenotypic, molecular sequencing, phylogenetic and computational approaches to evaluate the AdeB efflux pump as a potential therapeutic target in clinical Carbapenem-Resistant *A. baumannii* isolates (CRAB). **Results:** Among 354 clinical specimens collected from hospitalized adult patients in Najaf, Iraq, 47 *A. baumannii* isolates (13.3%) were identified and confirmed. Phenotypic susceptibility testing on all 47 isolates revealed high resistance rates across multiple antibiotic classes, including complete resistance to imipenem, gentamicin and amikacin (100%), as well as high resistance to cefepime (93.6%), meropenem (91.5%), and ciprofloxacin (82.9%). Overall, 43 isolates (91.5%) were classified as phenotypic carbapenem-resistant *A. baumannii* (CRAB), and 41 isolates (87.2%) were categorized as multidrug-resistant (MDR). A selected subset of 39 high-level CRAB isolates was subjected to molecular PCR analysis, revealing universal detection of the *AdeB* efflux pump gene (100%), alongside a widespread distribution of key resistance determinants including *blaOXA-51, blaOXA-23, IMP*, Class 1 integrons, and ESBL genes (*blaCTX, blaTEM,* and *blaSHV*). Sequencing and phylogenetic analysis of *AdeB* and *gyrB* genes demonstrated high sequence conservation and close evolutionary relatedness to global reference strains. The partial *Adeb* gene sequence generated in this study was deposited in the DNA Data Bank of Japan (DDBJ) under accession number LC918549. Three-dimensional structural modelling of the *AdeB* showed excellent stereochemical quality,

Creative Commons Attribution-Non-Commercial 4.0 International License

Published by DAC Democratic Arabic Center
DAC Democratic Arabic Center GmbH, Berlin

with 98.71% of residues located in Ramachandran favoured regions. Normal mode analysis confirmed flexibility and functional stability. **Conclusions:** Molecular docking identified strong binding affinities of efflux pump inhibitors, with Paβn showing the highest affinity **(-9.1 kcal/mol)** followed by the Pyridopyrimidine derivative **(–8.3 kcal/mol)**. Molecular dynamics simulations further validated the structural stability of AdeB, particularly at the 25 ns. Collectively, these finding support AdeB as a stable druggable target and highlight efflux pump inhibition as a promising strategy against multidrug-resistant *A. baumannii*.

Keywords: Bioinformatics analysis; Molecular Docking; Molecular dynamics simulations; Efflux pump (AdeB); Carbapenem-resistant *Acinetobacter baumannii* (CRAB); structure-based drug design; phylogenetic analysis; Efflux pump inhibitors and Pyridopyrimidine derivative.

1. Introduction

Acinetobacter baumannii is one of the most challenging nosocomial pathogens worldwide, notorious for causing severe infections such as pneumonia, bloodstream infections, urinary tract infections, and wound infections, particularly in intensive care units. Its ability to survive in harsh environments and resist multiple classes of antibiotics has made it a major global health concern [1,2]. According to the World Health Organization (WHO), *A. baumannii* is classified as a critical priority pathogen due to its high rate of multidrug resistance [3]. One of the primary mechanisms of resistance in *A. baumannii* is the overexpression of efflux pumps, especially those belonging to the Resistance Nodulation Division (RND) family. Among these systems, the AdeABC efflux pump plays a dominant role in mediating resistance to aminoglycosides, β-lactams, fluoroquinolones, tetracycline, and other antimicrobial agents [4]. The AdeB protein functions as the central transporter component of this tripartite system, facilitating the extrusion of a wide variety of substrates across the bacterial membrane [5]. Structural analyses have shown that AdeB possesses multiple substrate binding pockets that contribute to its broad substrate specificity and adaptability [6].

Due to the vital role of AdeB in antibiotic resistance, it represents a promising target for the design of efflux pump inhibitors (EPIs). These inhibitors can restore the efficacy of antibiotics by blocking substrate extrusion or altering the conformational dynamics of the transporter [7]. Among known EPIs, phenylalanine arginine β-

Creative Commons Attribution-Non-Commercial 4.0 International License

Published by DAC Democratic Arabic Center
DAC Democratic Arabic Center GmbH, Berlin

naphthylamide (PAβN) has been widely studied for its ability to inhibit RND efflux pumps, including AdeB, in gram negative bacteria. PAβN acts as a competitive inhibitor that binds within the substrate channel, preventing the efflux of antibiotics such as fluoroquinolones and β-lactams [8,9].

In recent years, bioinformatics and structure-based computational approaches have become valuable tools for investigating antimicrobial resistance mechanisms and supporting drug discovery. Among the components of the AdeABC efflux system, AdeB selected as the primary target in this study because it functions as the central transporter responsible for substrate recognition and extrusion and plays a major role in multidrug resistance in *A. baumannii*. Its high prevalence among carbapenem-resistance isolates and its suitability for structure-based analysis make it an attractive druggable target. Molecular docking enables the prediction of ligand binding orientation and affinities within target proteins, providing valuable insight into key interaction sites and energetic profiles [10-12]. Among the components of the AdeABC system, AdeB was selected as the primary target in this study because it functions as the central transporter responsible for substrate recognition and extrusion, playing a major role in multidrug resistance, its high prevalence among carbapenem-resistant isolates and suitability for structure-based analysis make it an attractive druggable target.

However, Despite the recognized importance of AdeB in multidrug resistance, comprehensive bioinformatics-driven analyses integrating phylogenetic tracking, structural modelling, molecular docking, molecular dynamics simulations, and normal mode analysis particularly utilizing locally characterized clinical isolates from endemic regional setting such as Iraq remain scarce. Furthermore, previous studies often evaluate genotypic presence without combining structural validation and dynamic stability profiles of local variants. To address this knowledge gap, it was hypothesized that AdeB variants circulating in local clinical setting maintain structural stability and druggable that can be therapeutically exploited. Therefore, this study aims to investigate the role and structural stability of the AdeB efflux pump in multidrug resistant *A. baumannii* clinical isolates from Al-Najaf, Iraq, using an integrated phylogenetic, molecular and computational framework. By combining local molecular characterization, DDBJ sequence deposition, homology modelling, molecular docking molecular dynamics simulations, and normal mode analysis, this work establish a

Creative Commons Attribution-Non-Commercial 4.0 International License

Published by DAC Democratic Arabic Center
DAC Democratic Arabic Center GmbH, Berlin

robust framework evaluating AdeB as a druggable target against carbapenem resistant *A. baumannii*.

2. Materials and Methods

2.1. Clinical Isolates and Patient Selection

A total of 354 non-duplicate clinical specimens (189 sputum samples, 73 blood samples, and 92 wound swabs) were collected from hospitalized patients admitted to tertiary care centres in Al-Najaf, Iraq, including Al-Sadder Medical City, between March and November 2024. The study cohort comprised adult patients (n=354; 126 males and 228 females) with ages ranging from 23 to 67 years. The inclusion criteria comprised adult inpatients presenting with clinical signs of hospital-acquired infection yielding pure primary microbial growth, whereas the exclusion criteria encompassed duplicate or recurrent isolates obtained from the same patient during the same hospitalization period to prevent epidemiological bias, specimens collected from outpatients, and contaminated samples or those with incomplete clinical records. To ensure epidemiological integrity, only the clinically relevant isolate per patient was included. Among the 354 collected specimens, 47 *Acinetobacter baumannii* isolates were identified and confirmed (Supplementary Table S1). All clinical isolates were processed initially in hospital laboratories and subsequently confirmed at the Molecular biology Postgraduate laboratory, Faculty of Medicine, University of Kufa. Species Identification was accomplished using morphological examination, microscopically evaluation, biochemical tests, CHROM agar Acinetobacter and Vitek 2 GN Compact System. The overall specimen distribution of the confirmed 47 isolates was as follows: Sputum (n=38, 80.9%), wound swabs (n=6, 12.7%), and blood cultures (n=3, 6.4%). All 47 confirmed *A. baumannii* isolates underwent phenotypic antimicrobial susceptibility profiling, and a representative subset of 39 high-level carbapenem-resistant *A. baumannii* (CRAB) isolates was selected to genomic DNA extraction and PCR screening of resistance determinants.

2.2. Bacterial Identification

The clinical sample (sputum, blood and wound samples) were cultured on MacConkey agar and blood agar and incubated at 37°C for 24 hours. Suspected *Acinetobacter* colonies were further sub cultured on Acinetobacter Chromogenic agar for preliminary identification. The isolates producing characteristic colonies on the compact system (bioMerieux, France) were identified as *Acinetobacter baumannii*. A

Creative Commons Attribution-Non-Commercial 4.0 International License

Published by DAC Democratic Arabic Center
DAC Democratic Arabic Center GmbH, Berlin

total 47 isolates were confirmed as *Acinetobacter baumannii* were selected for molecular analyses.

2.3. Antimicrobial Susceptibility Testing

Antimicrobial susceptibility testing was performed for all *Acinetobacter baumannii* isolates using the disk diffusion method on Muller Hinton agar (MHA) plates, following the guideline of the clinical and laboratory standards institute (CLSI M100,35th edition, 2025). Commercial antibiotic discs (Bioanalyses, Turkey) included imipenem (10ug), meropenem (10ug), gentamicin (10ug), amikacin (30ug), ciprofloxacin (5ug), ceftazidime (30ug), cefepime (30ug), and piperacillin/tazobactam (100/10ug). All plates were incubated at 37°C for 18-24h, and the zones of inhibition were measured in millimetres. The inhibition zone diameters were interpreted according to the Clinical and Laboratory Standards Institute (CLSI) guidelines (CLSI M100,35th edition, 2025) [13]. Isolates resistant to both imipenem and meropenem were classified as carbapenem resistant *A. baumannii* (CRAB). Multidrug resistance (MDR) was defined as resistance to at least one agent in three or more antimicrobial classes [14,15]. Therefore, MDR classification was based on the overall antimicrobial susceptibility profile rather than resistance to any single antimicrobial agent or class.

2.4. Detection of Efflux Pump and Resistance Genes

Genomic DNA was extracted from the *Acinetobacter baumannii* isolates using a commercial DNA extraction kit (Promega/USA) according to the manufacturer's instructions. To molecularly confirm species identification, all isolates were screened for the intrinsic ***blaOXA-51*** gene. Subsequently, a representative subset of 39 high-level carbapenem-resistant *A. baumannii* (CRAB) isolates was selected for comprehensive PCR screening of resistance determinants and efflux genes. The targeted genes included:

Efflux pump gene: *AdeB gene* was detected to evaluate the present of the AdeABC multidrug efflux system which, contributes significantly to the extrusion of antibiotics from *A. baumannii* bacteria; AdeB primer sequence (728bp) F" CCGGTATTACCTTTGCCGGA" R" TTGACCGCTTGAACCCATGA" at (30cycle) for (95°C for 2min, 95°C for 40sec, annealing at 59.8°C for 50sec,72°C for 50sec and 72°C for 5min) [16,17]

Carbapenemase and species-confirmation genes : (*blaOXA-51* and *blaOXA-23*) were screened as intrinsic species-confirmation markers and acquired β lactamase determinants conferring resistance to carbapenems, *blaOXA-51* primer sequence

Creative Commons Attribution-Non-Commercial 4.0 International License

Published by DAC Democratic Arabic Center
DAC Democratic Arabic Center GmbH, Berlin

(392bp) F "TAATGCTTTGATCGGCCTTG"/ R" TGGATTGCACTTCATCTTGG" and *blaOXA-23* primer sequence (465bp) F" GATCGGATTGGAGAACCAGA" /R"ATTTCTGACCGCATTTCCAT" at (30cycle) for (95°C for 2min, 95°C for 40sec, annealing at 54°C for 50sec,72°C for 50sec and 72°C for 5min) [15,18].

Metallo- β lactamase (MBL) genes: *IMP* was included to identify zinc- depended enzymes responsible for the hydrolysis of carbapenems, *IMP* primer sequence (587bp) F "ACCGCAGCAGAGTCTTTGCC" R " ACAACCAGTTTTGCCTTACC" at (30cycle) for (94°C for 2min, 94°C for 45sec, annealing at 44°C for 45sec,72°C for 45sec and 72°C for 5min).[19,20]

- **Integrons associated cassette genes**: *CS* and *Sul1* were amplified; CS represents the integron cassette sequence while sul confers sulfonamide resistance and often coexists within class1 integrons CS primer sequence (625bp) F " **GGCATCCAAGCAGCAAG" R " AAGCAGACTTGACCTGA"** at (30cycle) for (94°C for 3min, 94°C for 45sec, annealing at 52°C for 45sec,72°C for 45sec and 72°C for 5min) *Sul1* primer sequence (591bp) F " **CGGACGCGAGGCCTGTATC" R "GGGTGCGGACGTAGTCAGC"** at(30cycle) for (94°C for 3min, 94°C for 45sec, annealing at 54°C for 45sec,72°C for 45sec and 72°C for 5min) [21,22,23].
- **Extended spectrum - β lactamase (ESBL) gene: (***bla*$_{CTX-M}$, *bla*$_{TEM}$ and *bla*$_{SHV}$) were targeted to identify ESBL mediated resistance. The primer sequence and expected amplicon sizes were as follows: ***bla*$_{CTX-M}$ F " SCS ATG TGC AGY ACC AGT AA " and R " CCG CRA TAT GRT TGG TGG TG " yielding a (554 bp) product: for *bla*$_{TEM}$, F" TTTGGTATGGCTTCATTC" and R "AAAGATGCTGAAGATCA" yielding (425bp) product and for *bla*$_{SHV}$, F GGGTTATTCTTATTTGTCGC and R " TTAGCGTTGCCAGTGGTC" yielding (930bp)** product: the PCR thermocyclers' (30cycle) for (94°C for 3min, 94°C for 45sec, annealing at 52°C for 45sec,72°C for 45sec and 72°C for 5min [24].
- **The fluoroquinolone resistance gene:** *gyrB* encoding a subunit of DNA gyrase was analyzed to detect mutation associated with quinolone resistance. *gyrB* primer sequence (437bp) F "ACGGTATTGCTGTAGAAGTTGC" R "GCGTGTCATTTCACGTGCTT" PCR cycling condition by 30cycle of denaturation at 95°C for 2min, 95°C for 50sec, Annealing at 57°C for 50sec, extension at72°C for 50sec with final extension at 72°C for 5min) [16].

Creative Commons Attribution-Non-Commercial 4.0 International License

Published by DAC Democratic Arabic Center
DAC Democratic Arabic Center GmbH, Berlin

PCR amplification was performed in 25 ul reaction volumes containing 12.5 uL PCR Master Mix (Promega/USA) 1 uL of each primer (10uM), 3 uL of DNA template (50 ng/ul) and 7.5ul nuclease free water. PCR products were analyzed on 1.5% agarose gel stained with ethidium bromide and visualized under UV light. Amplified fragments sizes were compared with a 100bp DNA Ladder, and positive and negative isolates were included in each PCR run.

2.5. Sequencing and Analysis of *AdeB* and *GyrB*

The PCR products of *AdeB* and *gyrB* genes from Carbapenem resistance *Acinetobacter baumannii* isolates were purified using a PCR purification (Promega, USA) according to manufacturer's instruction and sent for Sanger sequencing to Microgen company, Korea. The resulting chromatograms were analysed to confirm the identity of the amplified fragments and to detect possible mutation associated with antibiotic resistance. Sequence data were processed using **BLASTn** (NCBI) to compare with reference sequences in GeneBank and multiple sequence alignments were performed using BLASTn/NCBI to detect genetic variation among isolates. Phylogenetic relationships were inferred using the Fast Minimum Evolution method to illustrate evolutionary clustering of *AdeB* and *gyrB* sequence. The sequencing results provided comprehensive insight into the conservation and diversity of these resistance determinants in clinical CRAB isolates from multiple hospitals in Najaf, Iraq. All sequences were submitted to NCBI/GeneBank with accession numbers. The sequenced AdeB PCR amplicon was further analysed using 279 aa AlphaFold model. This translated protein fragment was subsequently used for homology modelling and molecular docking analyses.

2.6. Phylogenetic Analysis of *AdeB* and *GyrB*

Phylogenetic analysis was conducted to assess the genetic relationship and diversity of the *AdeB* and *GyrB* sequences among CRAB isolates. Sequences were aligned using BLASTn/NCBI online platform, the Phylogenetic trees were constructed using NCBI Phylogenetic tool based on the Fast Minimum Evolution method. Branch reliability was assessed using bootstrap analysis (1000 replicates) and the resulting trees provided insights into the evolutionary clustering of the isolates and potential correlations with resistance profiles.

2.7. Protein Preparation

The translated amino acid sequence of the AdeB protein was submitted to the SWISS-MODEL server for homology modelling. The best template was automatically

Creative Commons Attribution-Non-Commercial 4.0 International License

Published by DAC Democratic Arabic Center
DAC Democratic Arabic Center GmbH, Berlin

selected based on the template quality, sequence identity, GMQE and QMEAN scores. The selected template was the efflux pump membrane transporter structure (PDB ID:7KGI, chain A: AdeB-ET-III), which exhibited 99.57% sequence identity and 100% sequence coverage with the target AdeB sequence. The generated model demonstrated high reliability, with a GMQE score of 0.88 and QMEAN score of 0.80± 0.05. the resulting 3D structure was evaluated for stereochemical quality and refined to remove steric clashes. Non-essential ligands, water molecules and heteroatoms were removed prior to molecular docking. The final prepared AdeB protein structure was saved in PDB format for downstream docking analysis [25,26]. The structural model used for docking analyses was generated from the sequenced AdeB fragment obtained in the present study rather than the full-length AdeB transporter. The selected template covered residues 1-2 79of the analysed AdeB sequence with 99.57% sequence identity and 100% coverage. Consequently, residue numbering reported in the docking analysis (e.g., ALA7, PHE8, and MET9) corresponds to positions within the modelled AdeB fragment and rather than the full-length AdeB protein.

2.8. Ligand (Compound) Preparation

The 2D chemical structure of the target ligands-specifically the known inhibitor PAβN dihydrochloride, the ChemSpider databases (ChemSpider ID: 28295746; SMILES: (Cl.Cl.N=C(N)NCCC[C@H](NC(=O)[C@@H](N)Cc1ccccc1)C(=O)Nc1ccc2ccccc2c1) and the Pyridopyrimidine derivative, the PubChem database (SCHEMBL 17560555; SMILES: CC1=C2C(=C(N(C1=O)C)NC3=C(C=C(C=C3)I)F)C(=O)N(C(=O)N2C4=CC=CC(=C4)NCC(=O)N)C) were retrieved from the retrieved from the ChemSpider and PubChem databases in MOL/SMILES format. The structure was converted into 2D/ 3D MOL2/PDBQT format using standard cheminformatics' tools. Energy minimization was performed using standard force field parameters. Both ligands were prepared by assigning correct protonation states, generating partial charges and defining rotatable bonds under physiological pH (7.4). The optimized ligand structure was saved and utilized as input configurations for subsequent docking simulations.

2.9. Protein-Ligand Docking Simulation

Molecular docking simulation were performed to predict the binding affinity and interaction pattern between the prepared AdeB protein model and the optimized ligand

Creative Commons Attribution-Non-Commercial 4.0 International License

Published by DAC Democratic Arabic Center
DAC Democratic Arabic Center GmbH, Berlin

structure (PaBn dihydrochloride). Docking was conducted using CB-Dock2 which provides automated cavity detection and flexible ligand docking. The processed protein structure (PDB format) and ligand files (MOL2/PDBQT) were uploaded and docking was executed under standard parameters. Binding pockets were automatically identified based on cavity volume and surface accessibility. The docking grid box dimensions were set to 26 x 26 x 26 Å, while sampling exhaustiveness was maintained to ensure reproducible and reliable scoring. The scoring used to include AC score and Vina based energy score, which allowed evaluation of binding affinity and selection of the most favourable docking conformation [27].

2.10. Binding Site Identification

The predicted binding pockets of the AdeB protein were analysed following the docking simulations. CB-Dock2 automatically identified potential cavities based on geometric features and protein surface topology. The top-ranked binding site was selected according to cavity volume, docking score and cluster consistency. Key amino acid residues contributing to ligand stabilization such as hydrogen bonding, hydrophobic interactions and electrostatic contacts were identified and mapped [27].

2.11. Visualization and Interaction Analysis of AdeB -PaBn

The docking result generated for the AdeB protein with the selected ligand PaBn dihydrochloride were visualized using Discovery Studio Visualizer (DSV). The software was employed to produce 2D and 3D interaction diagrams illustrating hydrogen bond donors and acceptors, hydrophobic interactions and electrostatic interactions. The visualization process allowed a detailed examination of the ligand orientation within the *AdeB* binding cavity including pocket depth, spatial positioning and conformational fit. The interaction patterns were analysed to describe the molecular interaction profile between AdeB and PaBn dihydrochloride.

2.12. Normal Mode Analysis (NMA) of AdeB Using iMODS

Normal mode analysis (NMA) of the AdeB efflux pump protein was performed using the iMODS server to predict intrinsic flexibility, global mobility, and potential deformation patterns under physiological conditions. The *AdeB* 3D structure (PDB format) was uploaded to the iMODS platform, which applies an internal coordinates elastic –network model to compute collective motions of the AdeB protein [28,29,30].

2.13. Molecular Dynamics (MD) Simulation of *AdeB* Efflux Pump

Molecular dynamics simulation was performed using the WebGRO platform for macromolecular simulation, which operates GROMACS molecular dynamics engine

Creative Commons Attribution-Non-Commercial 4.0 International License

Published by DAC Democratic Arabic Center
DAC Democratic Arabic Center GmbH, Berlin

[31,32]. The unbound target protein structure (Apo-form) was simulated using the GROMOS96 43a1 force field and the SPC water model within a triclinic simulation box. Non-protein components, including extraneous water molecules and heteroatoms, were excluded prior to setup. The systems were neutralized by adding Na+ and Cl- counter-ions to achieve a physiological salt concentration of 0.15 M NaCl. Energy minimization was performed using the Steepest Descent algorithm with 5000 steps to remove steric clashes and unfavourable contact. Following energy minimization, system equilibration was carried out under NVT and NPT ensembles at 300 K and 1 bar pressure. Production molecular dynamics simulations were subsequently performed using the Leap-frog integrator for 25 ns. The 25 ns simulation period represents the maximum duration supported by the WebGRO platform and was considered sufficient to evaluate the initial structural stability and conformational behaviour of the AdeB protein. Trajectory analyses included root mean square deviation (RMSD), root mean square fluctuation (RMSF), Radius of gyration (Rg), and solvent-accessible surface area/intramolecular hydrogen bonding. These parameters were utilized to evaluated the structural stability, compactness and conformational flexibility of the protein throughout the simulation trajectory.

2.14. Genetic and Statistical Analysis

The sequenced PCR products of target genes were analysed using NCBI/BLAST for sequence alignment and gene confirmation. Multiple sequence alignments and phylogenetic analyses were performed using NCBI/BLASTn to construct distance trees and identify conserved regions. Phylogenetic tree was visualized and annotated with NCBI Tree Viewer. Descriptive data were summarized as frequencies and percentages.

2.15. Ethics Approval

This study was conducted in accordance with the ethical principles of the Declaration of Helsinki and was approved by the Medical Ethics Committee, Faculty of Medicine, University of Kufa, Iraq (Approval No.MEC-168, approved on 19 May 2025). All procedures involving clinical samples were performed in compliance with institutional guidelines and patient confidentiality was strictly maintained throughout the study.

3. Results

3.1. Clinical Isolates and Identification of *Acinetobacter baumannii*

A total of 354 clinical samples collected from adults' patients admitted to different hospitals in Najaf/Iraq, forty-seven 47(13.3%) isolates were confirmed as

Creative Commons Attribution-Non-Commercial 4.0 International License

Published by DAC Democratic Arabic Center
DAC Democratic Arabic Center GmbH, Berlin

Acinetobacter baumannii following combination of morphological, microscopic, biochemical and CHROMO agar culture methods complemented by Vitek2 GN Compact system identification. The isolates were obtained from sputum, blood and wound swabs, with the sputum representing the predominant clinical source, highlighting the respiratory tract as important clinical *A. baumannii* among hospitalized patients. The isolate distribution across clinical specimens was as follows : 38 from Sputum (80.9%), 6 from wound swabs (12.7%), and 3 from blood cultures (6.4%). Initial identification using selective media and phenotypic assays was fully concordant with molecular confirmation, validating the accuracy of the diagnostic workflow for subsequent analyses.

3.2. Phenotypic Antimicrobial Susceptibility Patterns and Multidrug Resistance

Antimicrobial susceptibility testing was performed for all 47 confirmed *A. baumannii* isolates. High resistance rates were recorded across multiple antibiotic classes: imipenem (47/47,100%), meropenem (43/47, 91.5%), gentamicin (47/47,100%), amikacin (47/47,100%), ciprofloxacin (39/47, 82.9%), ceftazidime (40/47,85.1%) cefepime (44/47,93.6%) and piperacillin/tazobactam (40/47, 85.1%) (Supplementary Table S2). Based on phenotypic profiling, 43 out of 47 isolates (91.5%) exhibited dual resistance to both imipenem and meropenem, classifying them as carbapenem-resistant *A. baumannii* (CRAB). Furthermore, 41out of the 47 isolates (87.2%) were categorized as multidrug-resistance (MDR), exhibiting resistance to at least one agent in three or more antimicrobial categories. To evaluate the molecular underlying resistance determinants, a representative subset of 39 isolate displaying the highest phenotypic carbapenem resistance levels was selected from the CRAB cohort for subsequent PCR amplification and molecular characterization.

3.3. Molecular Detection of Efflux Pump and Resistance Genes

A selected subset of 39 highly resistant (CRAB) isolates (representing the core high-level carbapenem –resistant population) was subjected to molecular screening for resistance determinants. PCR analysis of the 39 carbapenem resistant *A. baumannii* (CRAB) isolates demonstrated a widespread distribution of multiple antibiotic resistance determinants. All targeted genes produced clear amplicons with the expected fragment sizes confirming the specificity and robustness of the molecular detection protocol: -

- **Efflux pump gene (*AdeB*):** The *adeB* gene (728bp) was detected in 100%(39/39) of the CRAB isolates, indicating universal expression of the AdeABC efflux pump

Creative Commons Attribution-Non-Commercial 4.0 International License

Published by DAC Democratic Arabic Center
DAC Democratic Arabic Center GmbH, Berlin

system. Its widespread presence highlights its major contribution to multidrug resistance as demonstrated in our study results.

- **Carbapenemase genes (*blaOXA-51 and blaOXA-23*):** The intrinsic *blaOXA-51* like gene (392bp) was present in 100%(39/39) of isolates consistent with its role as a molecular hallmark of *A. baumannii*. In contrast, the acquired *blaOXA-23* gene (465bp) was detected in 45%(18/39) of the CRAB isolates, reflecting its significant involvement in mediating carbapenem resistance.
- **Metallo-β-lactamase gene (*IMP*):** The *IMP* gene (587bp) was detected in 100%(39/39) of CRAB isolates, indicating universal carriage of this zinc dependent carbapenem hydrolysing enzyme and suggesting its key role in enhancing carbapenem resistance.
- **Integron associated cassette genes (*CS* and *sul1*):** The integron cassette genes *CS* (625bp) was present in 92%(36/39) of isolates, while the sulphonamide resistance gene *sul1* (591bp) was detected in 100%(39/39) of isolates. The high prevalence of these genes indicates extensive dissemination of class 1 integrons within the CRAB population.
- **Extended spectrum β-lactamase (ESBL) genes:** All three ESBL markers $bla_{CTX\text{-}M}$, bla_{TEM} and bla_{SHV} were detected in 100%(39/39) of the CRAB isolates, indicating widespread ESBL activity and supporting the observed resistance to third and fourth generation cephalosporins.
- **Fluoroquinolone Resistance gene (*gyrB*):** The fluoroquinolone resistance associated *gyrB* gene (437bp) was present in 100%(39/39) of the CRAB isolates, confirmed universal involvement of topoisomerase related resistance mechanisms, potentially through mutations within the quinolone resistance determining region (QRDR).

Overall, the molecular profile revealed a heavy burden of multidrug resistance determinants, fully consistent with the phenotypic resistance patterns and underscoring the clinical challenge posed by CRAB isolates.

3.4. Sequencing and Phylogenetic Analysis of *AdeB* and *GyrB* genes.

The PCR products of *adeB* and *gyrB* genes from CRAB isolates were successfully sequenced, yielding high quality chromatograms suitable for downstream analysis. Sequence alignment using NCBI/BLAST demonstrated that the sequenced *AdeB* and *gyrB* exhibited 97-100% sequencing identity with corresponding *A. baumannii* reference sequences confirming the identity of the amplified fragments.

Creative Commons Attribution-Non-Commercial 4.0 International License

Published by DAC Democratic Arabic Center
DAC Democratic Arabic Center GmbH, Berlin

***AdeB* gene:** Multiple sequence alignment revealed a high degree of conservation across the CRAB isolates, with minor nucleotide variations detected in a few positions. Phylogenetic analysis using the Fast Minimum Evolution method clustered the sequences into two main clades, reflecting slight genetic diversity among clinical isolates from different hospitals. The conservation of key functional regions suggests maintenance of efflux pump activity across the isolates.

***GyrB* gene:** The *gyrB* sequences demonstrated high conservation with reference sequence and minimal point mutations, potentially associated with fluoroquinolone resistance. Phylogenetic tree construction similarly showed clustering into two main lineages, consistent with geographical and clinical source variation. These finding indicate evolutionary stability of the *gyrB* gene while allowing minor sequence divergence, as illustrated in **Figure1**.

Overall sequencing and phylogenetic analyses confirmed the identity of the targeted resistance determinants and highlighted both the conserved and variable regions of *adeB* and *gyrB*, providing insight into the genetic relationships and evolutionary patterns among CRAB isolates in Najaf government.

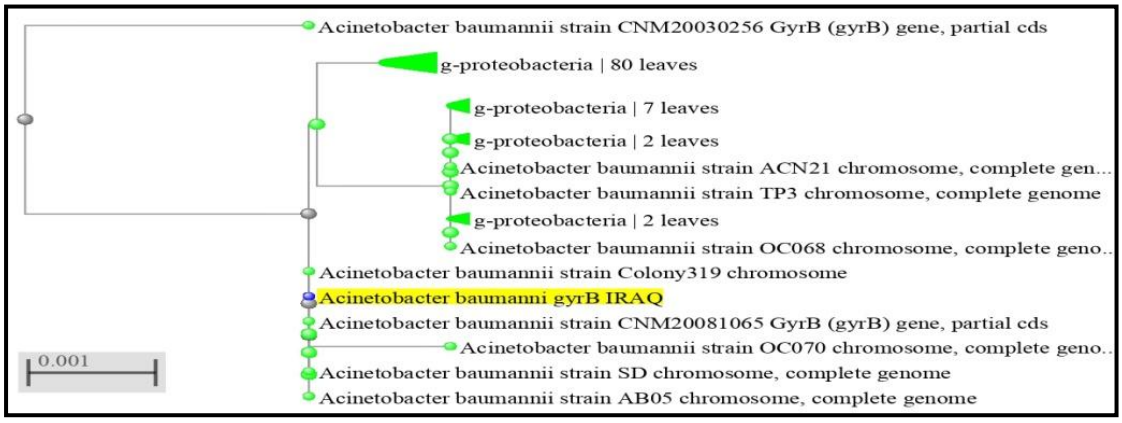


Figure 1. Phylogenetic Analysis of the Iraqi *gyrB* Gene Sequence Among Clinical *Acinetobacter baumannii* strains Using the NCBI Distance Tree Method.

The phylogenetic tree illustrates the evolutionary relationships of the *gyrB* gene sequence obtained from the clinical *Acinetobacter baumannii* isolates in this study (highlighted in yellow) compared with global reference strains retrieved from NCBI. The Iraqi *gyrB* sequence clustered closely with several well characterized *A. baumannii* strains, indicating a high degree of genetic similarity and suggesting the absence of major divergence within this resistance associated gene. The topology of the tree demonstrates two major clades. The tight clustering of the Iraqi strain, its close evolutionary proximity to international clinical isolates. The scale bar (0.001)

Creative Commons Attribution-Non-Commercial 4.0 International License

Published by DAC Democratic Arabic Center
DAC Democratic Arabic Center GmbH, Berlin

represents the estimated number of nucleotide substitutions per site, indicating low overall genetic distance and high conservation of the *gyrB* gene among *A. baumannii* populations.

3.5. Protein Structural Analysis and Modelling

3.5.1. Protein and ligand Visualization

The AdeB protein structure was visualized using both ribbon and surface-rendered 3D model to identify secondary structural elements and potential ligand-binding cavities (Figure 2A-B). The 2D chemical structures of Paβn dihydrochloride and Pyridopyrimidine derivative (SCHEMBL17560555) displayed key functional groups, hydrogen-bond donors/acceptors and rotatable bonds relevant to predicting ligand-protein interactions (Figures 2C-D).

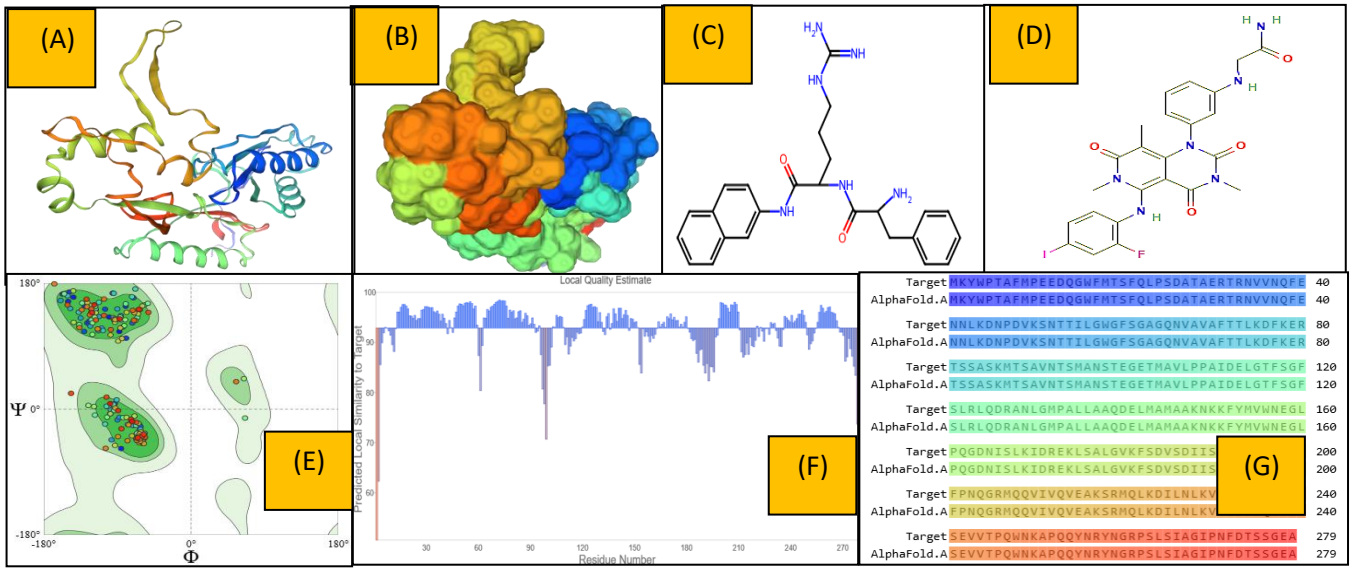


Figure 2. A-G: 3D Ribbon Representation of the AdeB Efflux Pump Protein Structure. B: Surface-rendered molecular model of the AdeB Efflux Pump Protein illustrating the solvent accessible topology and the location of potential ligand-binding cavities. C: 2D Chemical structure of Pyridopyrimidine derivative (SCHEMBL 17560555). D: 2D Chemical structure of the Paβn dihydrochloride compound. E. Ramachandran plot of AdeB efflux pump protein model. F. Local quality estimate of the predicted AdeB efflux pump protein model showing residue-level similarity to the target sequence. G. Multiple sequence alignment between the predicted AdeB protein model and the references sequence, showing conserved domains and residue-level consistency.

The model illustrates the overall folding architecture, including α-helices and β-strands forming the transmembrane and periplasmic domains. The structural

Creative Commons Attribution-Non-Commercial 4.0 International License

Published by DAC Democratic Arabic Center
DAC Democratic Arabic Center GmbH, Berlin

organization highlights regions potentially involved in substrate recognition and efflux transport, providing a structural basis for subsequent molecular docking analyses. Surface visualization reveals accessible grooves and pocket depressions across the protein exterior, corresponding to predicted docking cavities. These structural features define the spatial constraints and physicochemical environment surrounding the active binding sites targeted by PaBn and Pyridopyrimidine inhibitors. The 2D structural formula of Pyridopyrimidine derivative (SCHEMBL17560555) illustrates its heterocyclic scaffold, showing key functional groups, hydrogen-bond donors/acceptors, and ring-nitrogen positions relevant to its predicted binding interactions with AdeB efflux pump. In contrast, the 2D structure of Paβn dihydrochloride highlights its cationic amide chain and aromatic moieties, which contribute to hydrogen bonding and hydrophobic interactions within the AdeB binding cavity.

3.5.2. Ramachandran Plot and Structural Quality Assessment

The stereochemical quality of the predicted AdeB 3D structure was evaluated using the Ramachandran plot (Figure 2E) and MolProbity geometric parameters. The analysis showed that 98.71% of residues were positioned with favoured regions, with 0.00% Ramachandran outliers, demonstrating excellent backbone conformational geometry. Additionally, the structure contained 0.00% rotamer outlies, 0 C- beta deviations, and no bad bonds (0/1844). Only two minor angle deviations (2/2488) were detected at residues A171 (ASP) and the MET-PRO junction (A132-A133), both located in flexible loop regions.

These metrics collectively confirm the high stereochemical integrity of the AdeB model and support its suitability for downstream docking and molecular interaction analyses. The Ramachandran plot illustrates the distribution of φ (phi) and ψ (psi) backbone dihedral angles for all residues in the predicted AdeB 3D model. The majority of residues fall within the favoured and allowed regions, indicating good stereochemical quality and supporting the overall structural validity of the homology model. In contrast, The local quality estimate plot represents the pre-residue predicted similarity to the target sequence. Most residues display high predicted similarity (>90%), reflecting strong structural reliability. Minor decreases correspond to flexible loop regions, which commonly exhibit reduced modelling confidence. These results support the robustness and accuracy of the predicted AdeB structure.

Creative Commons Attribution-Non-Commercial 4.0 International License

Published by DAC Democratic Arabic Center
DAC Democratic Arabic Center GmbH, Berlin

3.5.3. Sequence Alignment and Structural Consistency Analysis

Multiple sequence alignment was performed between the predicted AdeB 3D structure and the reference amino acid sequence to assess sequence –structure agreement (Figure2G). The alignment revealed complete residue level conservation across the entire protein length, indicating that the modelled structure accurately reflects native AdeB sequence. No amino acid substitutions, insertions, or deletions were detected between the modelled AdeB sequence and the reference sequence, confirming complete sequence identity and structural consistency. Conserved regions, domains, and functionally important motifs were consistently preserved in both the model and the target sequence. This high level of alignment consistency supports the structural reliability of the predicted AdeB model and confirms its suitability for subsequent docking and molecular dynamic analyses. The multiple sequence alignment compares the predicted AdeB protein (AlphaFold model) with the references target sequence. The high degree of residue conservation across the entire length of protein indicates strong sequence-structure agreement. Conserved motifs appear in identical colour blocks, demonstrating accurate modelling of functionally important regions and confirming the reliability of the predicted AdeB structure.

3.6. Molecular Docking of AdeB with PaBn and Pyridopyrimidine Inhibitors

3.6.1. Docking of AdeB with PaBn Inhibitor

PaBn was successfully docked into the predicted binding pockets of AdeB efflux pump. Among the identified cavities, C2 exhibited the lowest Vina binding energy of **(–9.1 kcal/mol)** representing the most thermodynamically favourable interaction. This pocket showed a cavity volume of **305Å** and was cantered at coordinates (10, -7, -17). The docking grid box dimensions (26 x 26 x 26 **Å**) ensured complete inclusion of the ligand within the active site. Other predicted pockets (C1, C3, C4 and C5) demonstrated higher binding energies (-8.4, -8.2, -7.1 and -8.5 kcal/mol, respectively), confirming C2 as the optimal binding cavity and the primary site selected for detailed interaction analysis.

Key residues forming the C2 binding pocket included: **Chain A**: ALA7 PHE8 MET9 PRO10 GLU11 GLU12 ASP13 SER83 ALA84 SER85 LYS86 THR88 SER89 ASN92 ALA105 VAL106 LEU107 PHE117 SER118 GLY119 TYR153 ILE269 PRO270 ASN271 PHE272 ASP273 THR274 SER275 SER276.

Molecular interaction analysis revealed:

Creative Commons Attribution-Non-Commercial 4.0 International License

Published by DAC Democratic Arabic Center
DAC Democratic Arabic Center GmbH, Berlin

Hydrogen bonds: SER83, SER85, THR88 and ASP13, stabilizing the ligand within the pocket.

Hydrophobic interactions: PHE8, LEU107 and PHE117 reinforcing the ligand- protein interface.

Electrostatic contacts: GLU11 and GLU12 further supporting overall binding stability. DSV visualization provided detailed 2D and 3D interaction profiles, showing: Precise orientation and positioning of PaBn within the cavity. Adequate pocket depth and structural complementarity, suggesting the ligand's potential to obstruct the efflux channel. Clear mapping of functional residues essential for AdeB efflux pump activity (Figures 3A-D).

Overall, these results demonstrate the strong binding affinity of PaBn toward AdeB, reinforcing its potential as an efflux pump inhibitor. The alignment between binding energy, interacting residues, and ligand orientation underscores the robustness and reliability of the docking simulation (Table.1).

Table 1. Summary of the top predicted AdeB binding pockets for PaBn based on CB-dock2 results, including Vina binding scores, cavity volumes, pocket centres and docking box dimensions.

CurPocket ID	Vina score	Cavity volume (Å^3)	Centre (x, y, z)	Docking size (x, y, z)	Template
C2	-9.1	305	10, -7, -17	26, 26, 26	NA
C5	-9.0	112	21, 1, -11	26, 26, 26	NA
C3	-8.3	236	2, -8, -13	32, 26, 35	NA
C1	-8.2	3956	2, -8, -13	32, 26, 35	NA
C4	-6.6	209	-8, 3, 18	26, 26, 26	NA

Creative Commons Attribution-Non-Commercial 4.0 International License

Published by DAC Democratic Arabic Center
DAC Democratic Arabic Center GmbH, Berlin

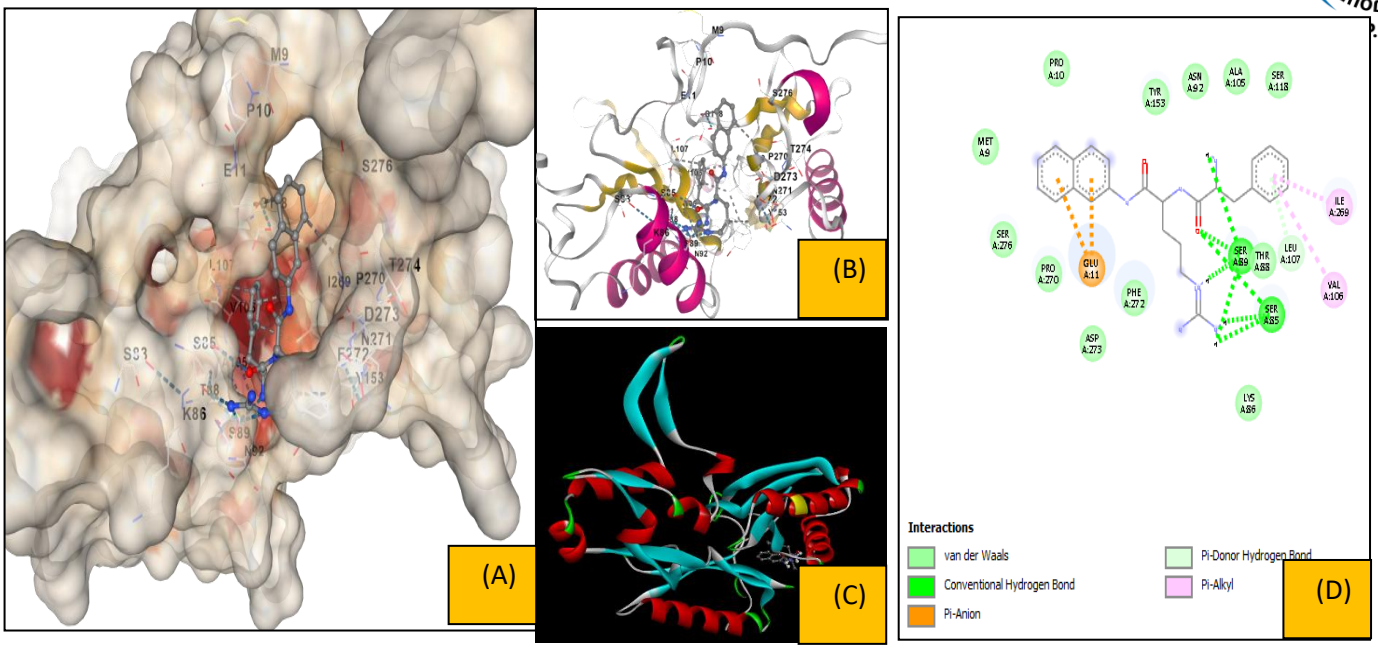


Figure 3. A. Surface-rendered representation of the AdeB binding pocket (C2) showing PaBn positioned within the cavity and surrounded by key interacting residues. B. Ribbon model of AdeB illustrating the structural context of cavity C2 and the precise orientation of PaBn within the binding site. C: 3D interaction visualization showing hydrogen bonding, hydrophobic contacts and electrostatic interactions between PaBn and AdeB residues. D: 2D interaction map of PaBn within the AdeB pocket (C2), highlighting all relevant hydrogen bonds, hydrophobic and pi-type contacts.

3.6.2. Docking of AdeB with Pyridopyrimidine Inhibitor

Pyridopyrimidine (Pyri) was successfully docked into the predicted binding pockets of AdeB efflux pump. Among all identified pockets, C1 exhibited the lowest Vina binding energy of **(–8.3 kcal/mol),** indicating the most thermodynamically favourable interaction site. Pocket C1 possessed a cavity volume of **3956Å^3** and was cantered at coordinates (2, -8, -13). The docking grid box (32 x 24 x 35 **Å**) provided complete spatial coverage for Pyri, ensuring optimal placement within the binding cavity. Other pockets (C2, C3, C4 and C5) showed comparatively higher binding energies (-8.2, -7.5, -7.4, and 7.8 kcal/mol, respectively), further confirming C1 as the primary and most favourable binding location, Key residues forming the C1 binding pocket included: **Chain A**: THR6 ALA7 PHE8 MET9 PRO10 GLU11 PRO109 ALA110 ILE111 LEU114 GLY115 THR116 PHE117 SER118 GLY119 PHE120 SER121 LEU122 ARG123 PHE152 TYR258 GLY268 PRO270 THR274 SER276 GLY277 ALA279.

 Creative Commons Attribution-Non-Commercial 4.0 International License Published by DAC Democratic Arabic Center
DAC Democratic Arabic Center GmbH, Berlin

Major molecular interactions categories identified within the primary pocket (C1):

Hydrogen bonds: THR6, THR116, SER118, contributing to ligand stabilization within the cavity.

Hydrophobic interactions: PHE8, LEU114, PHE117, strengthening ligand – protein complementarity.

Electrostatic contacts: GLU11, ARG123, reinforcing overall binding stability.

DSV visualization confirmed the docking results, providing detailed 2D and 3D interaction maps, revealing:

Accurate positioning and orientation of Pyri within the C1 pocket.

Adequate cavity depth and shape complementarity, supporting its potential to obstruct the efflux channel.

Mapping of functional residues involved in ligand binding and AdeB efflux pump transport activity (Figures 4A-D). Overall, these findings demonstrate that **Pyridopyrimidine exhibits strong** and favourable binding affinity toward AdeB, supported by consistent docking energy, stable interactions profiles, and proper conformational fit within the C1 pocket. The coherent agreement between binding score, residues-level contacts and ligand orientation validates the reliability of the docking simulation (Table.2).

Table 2. Docking pocket characteristics and binding energies of the Pyridopyrimidine inhibitor within the AdeB efflux pump, including Vina score, cavity volumes, spatial coordinates and grid box dimensions.

CurPocket ID	Vina score	Cavity volume (Å^3)	Centre (x, y, z)	Docking size (x, y, z)	Template
C1	-8.3	3956	2, -8, -13	32, 24, 35	NA
C2	-8.2	305	10, -7, -17	24, 24, 24	NA
C5	-7.8	112	21, 1, -11	24, 24, 24	NA
C3	-7.5	236	-6, -10, -2	24, 24, 24	NA
C4	-7.4	209	-8, 3, 18	24, 24, 24	NA

Creative Commons Attribution-Non-Commercial 4.0 International License

Published by DAC Democratic Arabic Center
DAC Democratic Arabic Center GmbH, Berlin

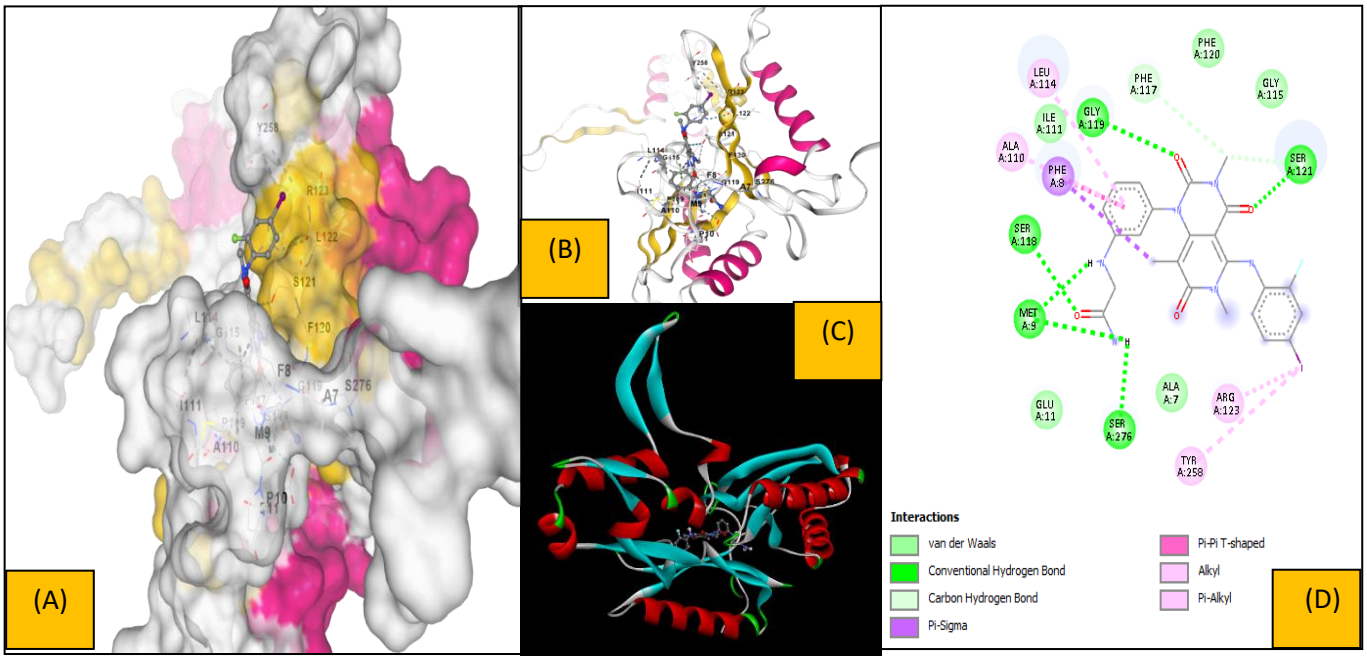


Figure 4. A. Surface-rendered visualization of the AdeB C1 binding pocket highlighting the embedded Pyridopyrimidine ligand and the surrounding pocket topology. B. Ribbon representation of the AdeB efflux pump showing the overall 3D orientation and binding position of the Pyridopyrimidine inhibitor within the C1 pocket. C. 3D interaction map showing hydrogen bonding, hydrophobic contacts and electrostatic interactions between Pyridopyrimidine and key residues within the AdeB C1 pocket. D. 2D interaction map (LigPlot+) illustrating van der Waals forces, hydrogen bonds, ╥-interactions and key residue contacts stabilizing Pyridopyrimidine within the AdeB C1 binding pocket.

3.6.3. Comparative Docking Analysis of PaBn and Pyridopyrimidine Inhibitors

Both PaBn and Pyri demonstrated effective binding to AdeB efflux pump; however, PaBn exhibited slightly higher affinity (-9.1 kcal/mol) compared to Pyri (-8.3 kcal/mol), including superior inhibitory potential. The comparative analysis revealed the following key observations: **Critical interacting residues**: Both ligands engaged essential amino acids within their respective binding pocket through hydrogen bonding, hydrophobic contacts, and electrostatic interactions. These interactions collectively contributed to ligand stabilization and pockets occupancy. **Molecular interactions patterns: PaBn** formed a denser interactions network-particularly hydrogen bonds, hydrophobic interactions, and electrostatic contacts-supporting its stronger affinity. Pyri also displayed stable interactions, through slightly fewer, suggesting effective but

Creative Commons Attribution-Non-Commercial 4.0 International License

Published by DAC Democratic Arabic Center
DAC Democratic Arabic Center GmbH, Berlin

comparatively moderate inhibition of the efflux activity. **Structural complementarity and ligand positioning**: DSV visualization 2D and 3D interaction maps confirmed optimal ligand orientation, pocket complementarity, and residues essential for AdeB function. Overall, docking results indicate that both compounds are representing promising inhibitors targeting the AdeB efflux pump, however; PaBn demonstrating slightly stronger binding affinity, richer interaction network and more a favourable conformational fit, supporting its potential as a lead candidate for inhibiting AdeB mediated multidrug resistance in *Acinetobacter baumannii* isolates.

3.7. Normal Mode Analysis (NMA) of *AdeB* Using iMODS

The intrinsic dynamics, stability and structural flexibility of *AdeB* efflux pump were evaluated using normal mode analysis (NMA) via the iMODS server. The results provide detailed insights into collective motions, deformability, residue correlations and energy requirements with structural transitions of the protein.

Deformability Profile

The deformability plot illustrates the flexible and rigid regions along the AdeB structure (Figure 5A). Peaks indicate residues with higher mobility, typically corresponding to loop segments, whereas the overall moderate deformability suggests a stable global fold with limited localized fluctuations.

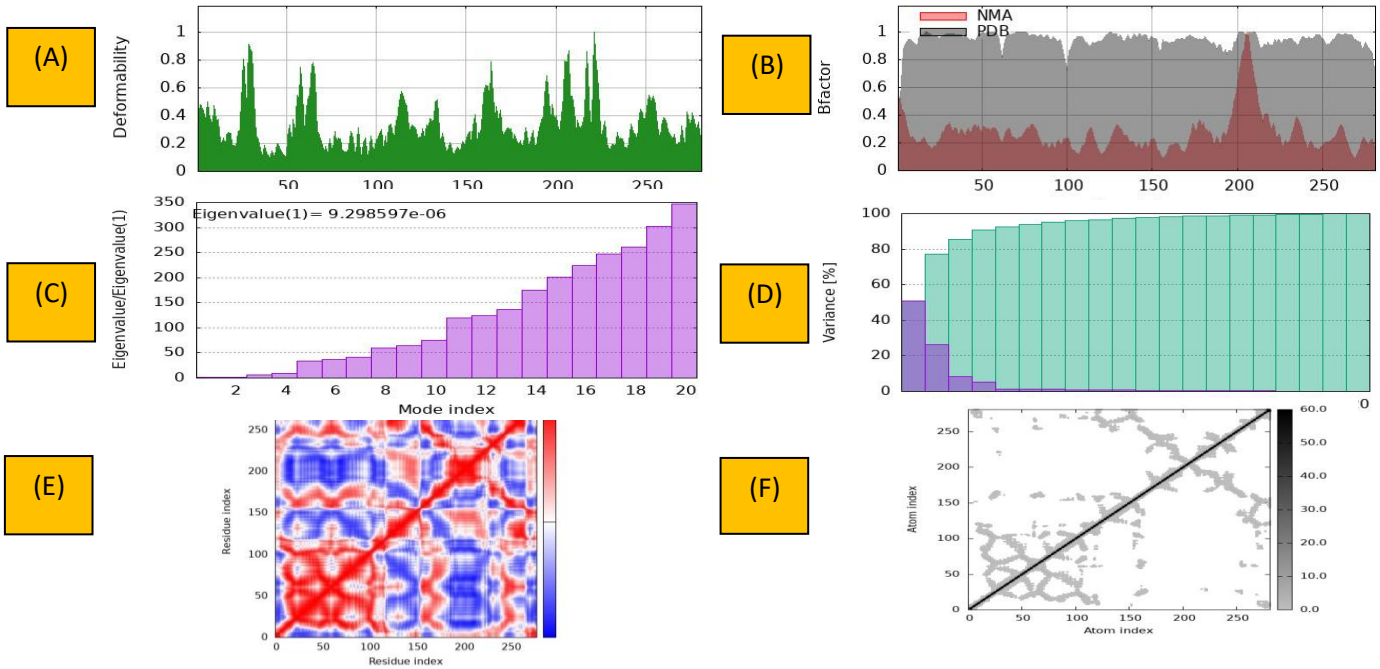


Figure 5. A. Deformability plot of AdeB efflux pump showing residue-level flexibility based on NMA analysis. **B.** NMA derived B-factor profile compared with PDB

Creative Commons Attribution-Non-Commercial 4.0 International License

Published by DAC Democratic Arabic Center
DAC Democratic Arabic Center GmbH, Berlin

mobility values, indicating structural stability. **C.** Eigenvalue distribution of the first 20 normal modes highlighting motion stiffness of AdeB. **D.** Variance plot showing the contribution of each normal mode to the total motion. E. Covariance matrix illustrating correlated (red) and anti –correlated (blue) motions within AdeB. F. Elastic network model demonstrating inter –residue connection strength and structural rigidity

B-factor (Mobility) analysis: The NMA derived B- factor profile (Figure 5B) closely mirrored the PDB-based B-factor distribution, confirming consistency between the modelled structure and its predicted dynamic behaviour. Most residues exhibited low mobility, with minor increase in exposed loop regions, reflecting a stable conformation suitable for ligand accommodation.

Eigenvalue and Motion Stiffness: The eigenvalue associated with the first internal mode was 9.298597e-06, indicating low energy is required for collective conformational motion (Figure 5C). Lower eigenvalue implies easier deformation, which is advantageous for functional transitions such as ligand binding and efflux-channel opening

Variance and mode Distribution: The variance plot (Figure 5D) shows that the first few modes contribute the most to total motion, while higher modes account for finer local movement. This confirms that AdeB exhibits well-defined collective dynamics typical of transporter proteins.

Covariance Matrix: The covariance matrix (Figure 5E) revealed correlated (red), anti-correlated (blue), and uncorrelated (white) motions among residue pairs. Strongly correlated blocks indicate coordinated domain movement essential for substrate transport, while anti –correlated regions highlight hinge –like behaviour within the protein structure.

Elastic Network Model: The elastic network graph (Figure 5F) indicates the strength of inter –residue connections, where darker nodes reflect stiffer interactions. The dense network connectivity across the protein suggests mechanical stability and efficient transmission of conformational change during efflux activity.

3.8. Molecular Dynamic Simulation Analysis of *AdeB* Efflux Pump Using GROMACS

A molecular dynamics (MD) simulation was initially performed for 1 ns to investigate the structural stability, compactness, flexibility, and solvent exposure of the AdeB efflux pump of *Acinetobacter baumannii* isolates in aqueous environment. The trajectory analysis included RMSD, RMSF, radius of gyration (Rg), hydrogen bonding

Creative Commons Attribution-Non-Commercial 4.0 International License

Published by DAC Democratic Arabic Center
DAC Democratic Arabic Center GmbH, Berlin

profile, solvent accessible surface area (SASA), and residue-wise surface area distribution.

To further validate the dynamic behaviour of AdeB and assess the impact of simulation length on structural convergence, additional MD simulation of 10 ns and 25 ns were subsequently conducted under identical simulation conditions. Comparative analysis across the three-time scale (1 ns, 10 ns, 25 ns) enabled a more robust evaluation of long-term conformational stability and equilibration behaviour. The extended 25 ns simulation exhibited enhanced RMSD convergence, reduced structural fluctuations, stabilized radius of gyration, and more consistent hydrogen-bonding and solvent exposure profiles, indicating superior equilibration and dynamic reliability compared to shorter trajectories. These finding demonstrate that longer MD simulations provide a more realistic representation of AdeB conformational dynamic and justify the use of the 25 ns trajectory as the primary reference for structural stability assessment and comparative analysis.

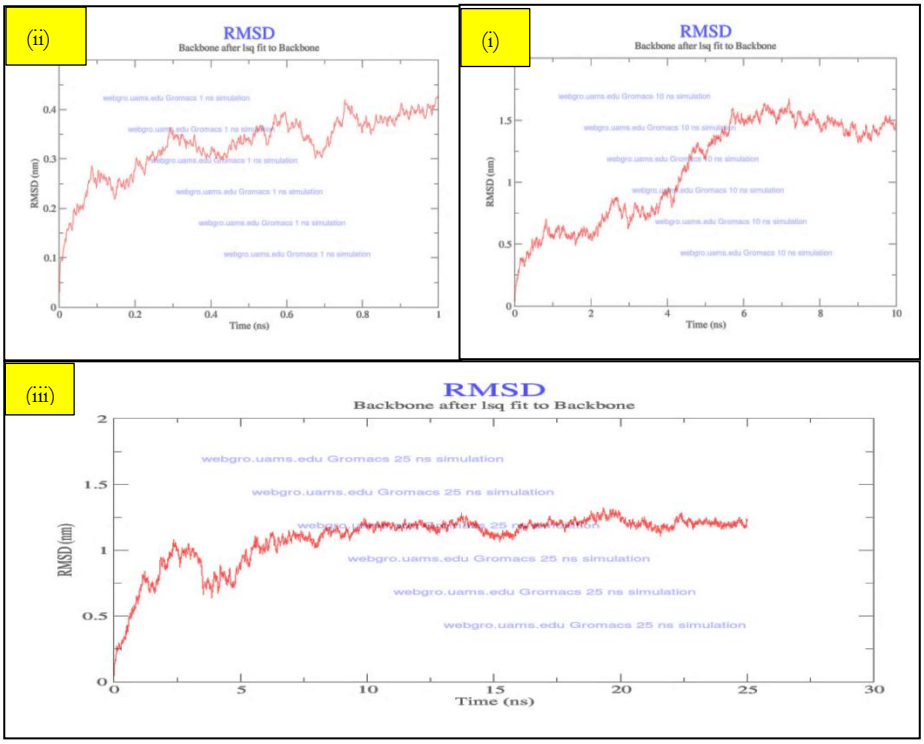
3.8.1. Root Mean Square Deviation (RMSD) of the AdeB

The backbone RMSD of the AdeB efflux pump exhibited a gradual increase from approximately 0.10 nm at the initial stage to ~0.42 nm within the first 1 ns of simulation, indicating early structural relaxation and equilibration. Extension of the simulation to 10 ns resulted in a further increase in RMSD, reaching an average range of ~1.4-1.6 nm, followed by partial stabilization, reflecting enhanced conformational sampling and adaptation of the protein backbone. Notably, during the extended 25 ns simulation, the RMSD profile converged to a more stable plateau around ~1.2-1.3 nm with reduced fluctuation, demonstrating long-term structural equilibration and sustained backbone stability. The progressive stabilization observed across increasing simulation times confirms that AdeB achieves a dynamically stable conformation under aqueous conditions, with the 25 ns trajectory providing the most reliable representation of its equilibrium behaviour (Figure 6A (i-iii).

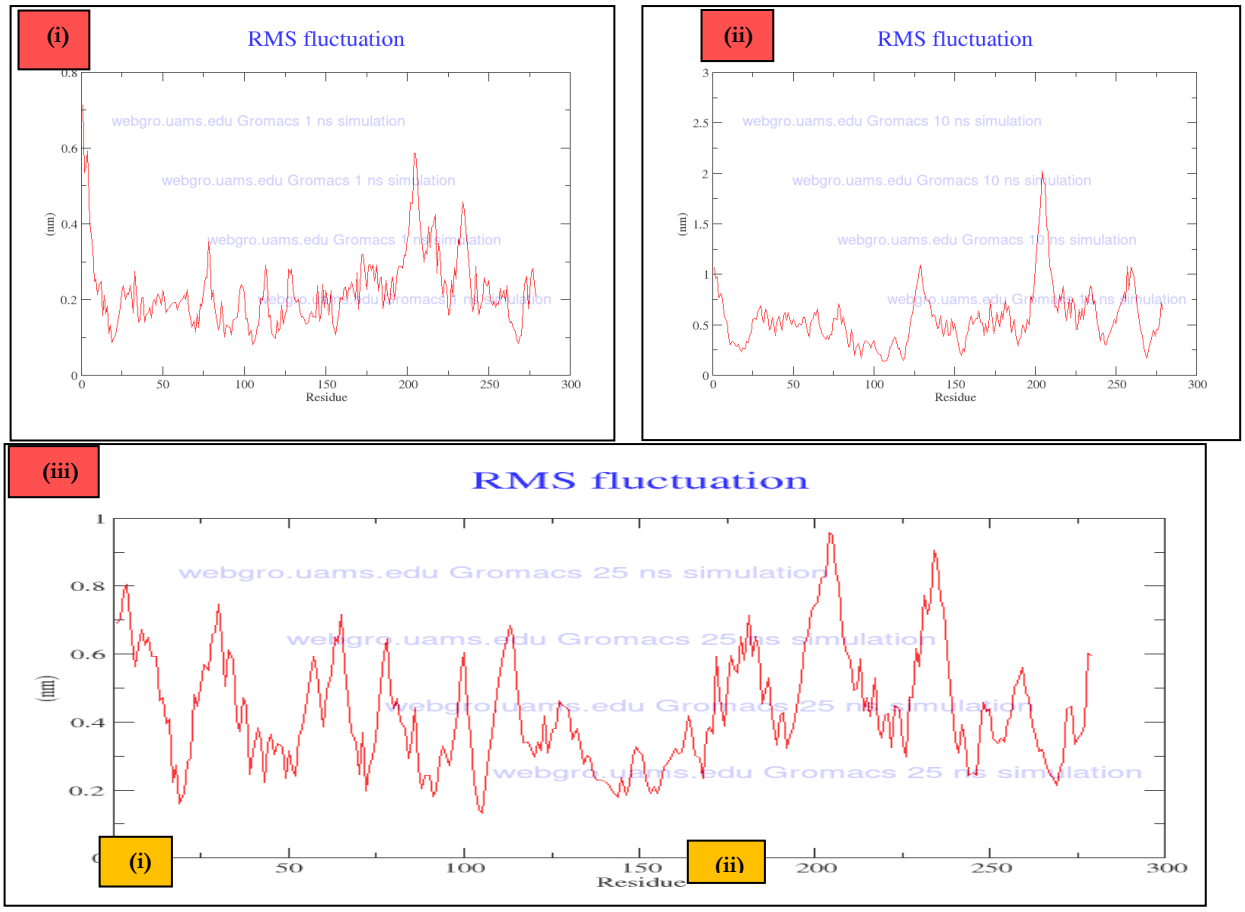
Creative Commons Attribution-Non-Commercial 4.0 International License

Published by DAC Democratic Arabic Center
DAC Democratic Arabic Center GmbH, Berlin

(A)



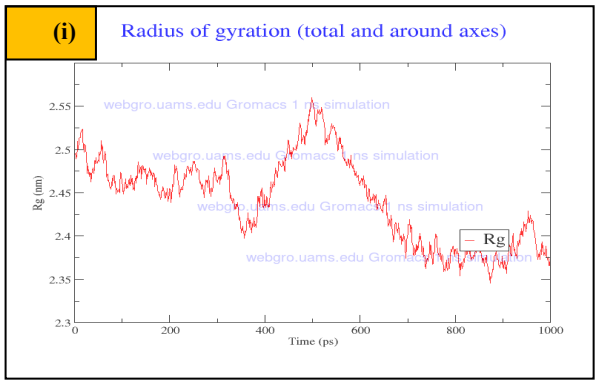
(B)

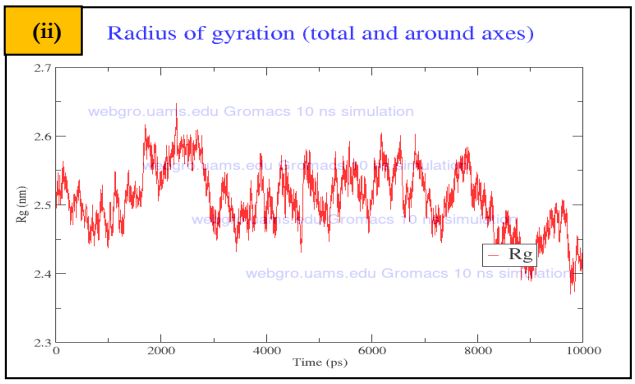


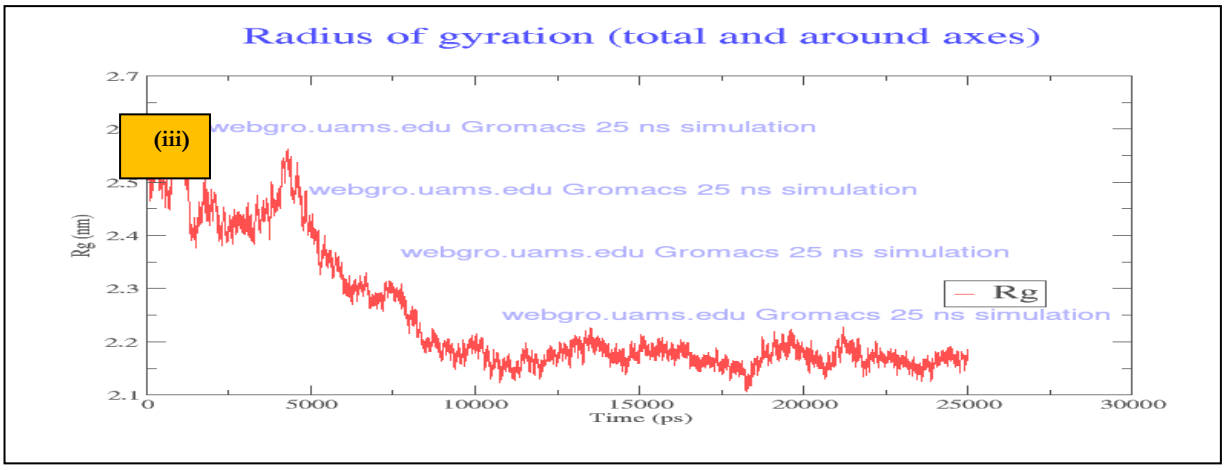
Creative Commons Attribution-Non-Commercial 4.0 International License

Published by DAC Democratic Arabic Center
DAC Democratic Arabic Center GmbH, Berlin

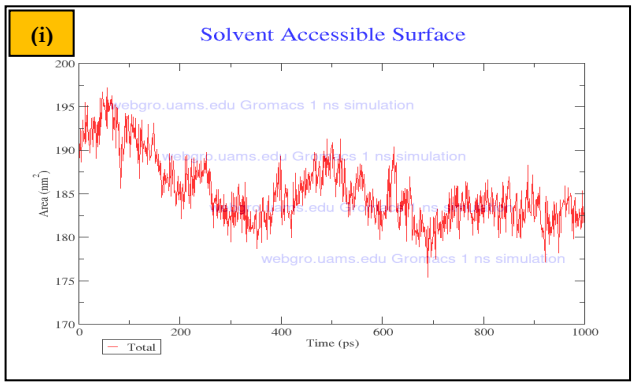
(C)

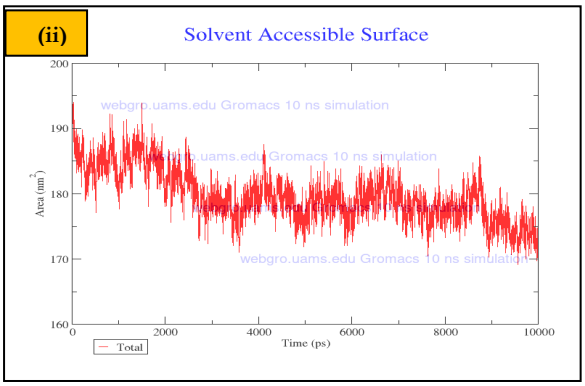


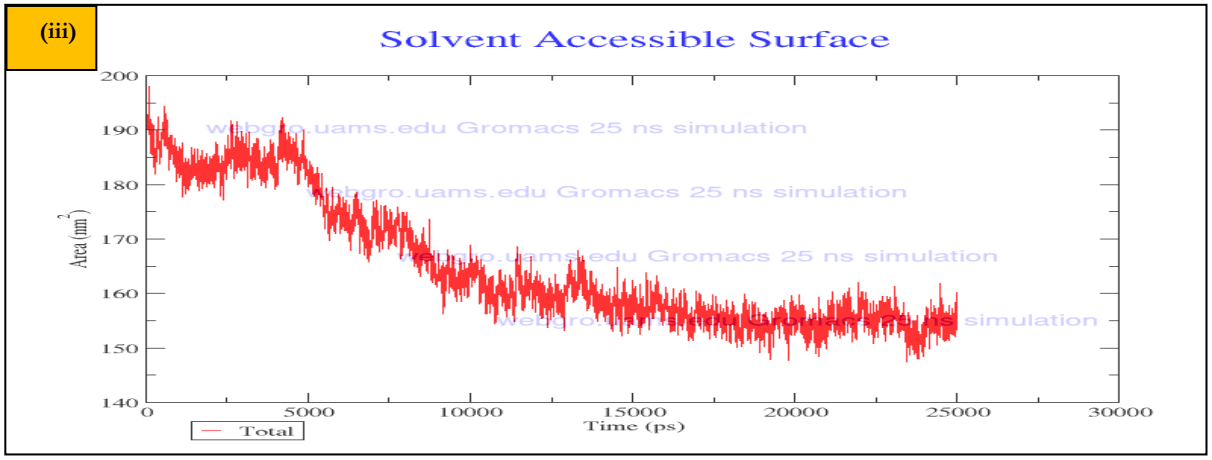




(D)



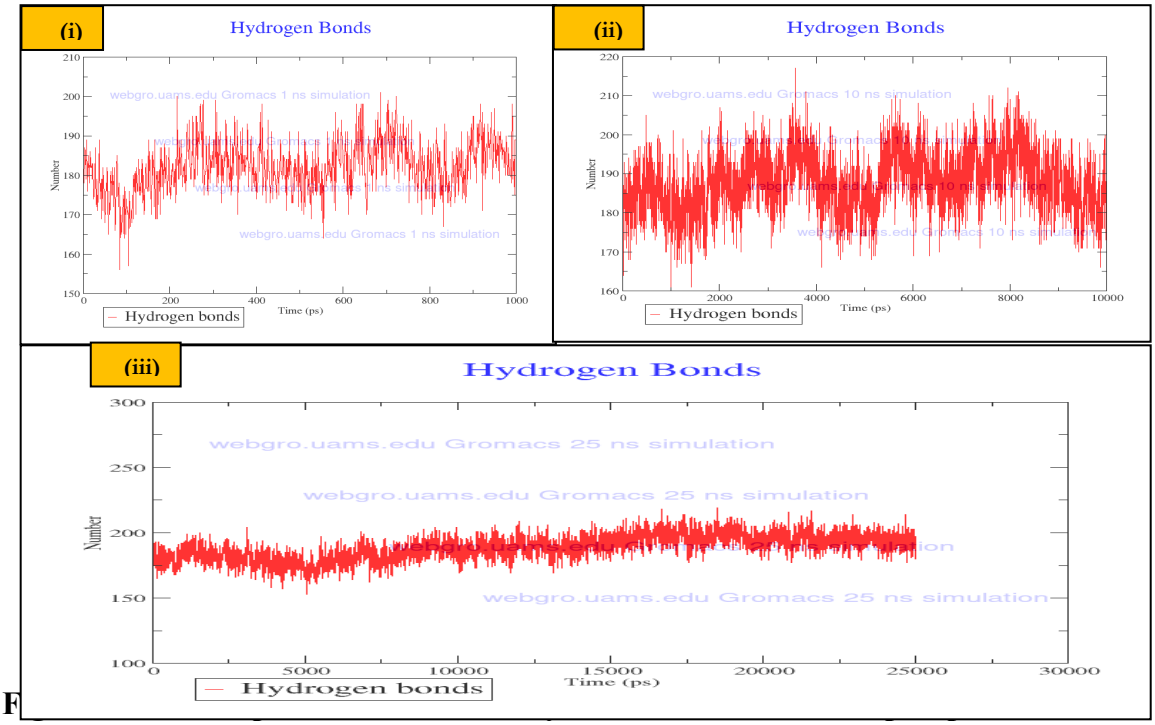




Creative Commons Attribution-Non-Commercial 4.0 International License

Published by DAC Democratic Arabic Center
DAC Democratic Arabic Center GmbH, Berlin

(E)



F

across different MD simulation times. (i) *RMSD profile over 1ns, showing initial structural equilibration with gradual stabilization. (ii) RMSD profile over 10 ns, indicating increased conformational sampling and partial stabilization. (iii) RMSD profile over 25 ns, demonstrating sustained RMSD convergence and long-term backbone stability of AdeB. Collectively, the comparative confirm that extended simulation (25ns) provides a more reliable and realistic assessment of AdeB backbone stability than shorter trajectories.* **6B(*i-iii*). Comparative RMSF analysis of the AdeB efflux pump across different Molecular dynamic simulation times using GROMACS. (i)** *RMSF profile over a 1ns MD simulation, showing moderate flexibility primarily localized to terminal and loop regions. (ii) RMSF profile over a 10 ns MD simulation, indicating increased residue –wise fluctuations reflecting enhanced conformational sampling. (iii) RMSF profile over a 25 ns MD simulation, demonstrating reduced fluctuation amplitudes and improved dynamic stabilization of the protein backbone. The comparative RMSF profile illustrate a clear time –dependent refinement of local flexibility, with extended simulation time (25 ns) results in a more equilibrated and physiologically relevant dynamic behavior of the AdeB efflux pump.* **C (i-iii). Comparative radius of gyration (Rg) analysis of the AdeB efflux pump across different MD simulation times using GROMACS. (i)** *Rg profile over 1 ns simulation, showing stable global compactness with minor transient fluctuations. (ii) Rg profile over 10 ns MD simulation, indicating increased conformational sampling*

Creative Commons Attribution-Non-Commercial 4.0 International License

Published by DAC Democratic Arabic Center
DAC Democratic Arabic Center GmbH, Berlin

while maintaining structural integrity. (iii) Rg profile over 25 ns MD simulation, demonstrating reduced Rg values and enhanced compactness, reflecting improved equilibration and long-term structural stabilization of the AdeB efflux pump. **D (*i-iii*). Comparative solvent accessible surface area (SASA) analysis of the AdeB efflux pump across different MD simulation times using GROMACS.** *(i)*- SASA profile over 1-ns MD simulation showing early surface rearrangement and partial compaction. *(ii)*- SASA profile over 10-ns MD simulation indicating increased conformational sampling and intermediate stabilization. *(iii)*- SASA profile over 25-ns MD simulation demonstrating sustained reduction in solvent exposure and enhanced structural compactness. The comparative SASA profiles indicate time dependent stabilization with extended simulation (25 ns) results the most compact and equilibrated conformation of AdeB. **E(i-iii). Comparative hydrogen bond analysis of the AdeB efflux pump during molecular dynamics simulations using GROMACS. (i)** Hydrogen bond profile over 1 ns MD simulation showing moderate fluctuations during initial equilibration. (ii) Hydrogen bond profile over 10 ns MD simulation indicating increased hydrogen bond density associated with enhanced conformational sampling. (iii) Hydrogen bond profile over 25 ns MD simulation, demonstrating stabilized hydrogen bonding patterns and improved intramolecular cohesion. The comparative analysis time dependent refinement of the hydrogen bonding network, with extended simulation (25 ns) results a more equilibrated and structurally stable AdeB conformation.

3.8.2. Root Mean Square Fluctuation (RMSF) Plot Analysis for AdeB

The residue –wise RMSF analysis (Figure 6B) was employed to evaluate the local dynamic flexibility of the AdeB efflux pump across different molecular dynamic simulation times (1 ns, 10 ns, 25 ns) providing insight into time-dependent conformational behaviour: During the 1-ns simulation, AdeB exhibited characteristic flexibility patterns with elevated fluctuations observed in N-terminal region (first ~20 residues; 0.60-0.70 nm) consistent with terminal or loosely structured segments. In contrast, the core structural domains maintained low RMSF values (0.15-0.30 nm) indicating pronounced rigidity and preservation of secondary structural elements. A moderately flexible region spanning residues ~180-230 showed RMSF values of approximately 0.50- 0.60 nm, corresponding to surface –exposed loop regions involved in functional adaptability. Extension of the simulation to 10 ns revealed an increase in residue-wise fluctuations, particularly within loop and surface-accessible regions, with

Creative Commons Attribution-Non-Commercial 4.0 International License

Published by DAC Democratic Arabic Center
DAC Democratic Arabic Center GmbH, Berlin

RMSF peaks exceeding those observed at 1 ns. This behaviour reflects enhanced conformational sampling and transitional flexibility as the protein explores a broader conformational space before full equilibration. In contrast, the 25-ns simulation demonstrated a refined and stabilized RMSF profile, characterized by reduced fluctuation amplitudes across most residues and confinement of higher mobility to specific functional loop regions. The persistence of low RMSF values within the protein core confirms improved structural equilibration and long-term dynamic stability, indicating that the AdeB efflux pump reached a more physiologically relevant conformational state at extended simulation time. Overall, the comparative RMSF profiles highlight a clear time-dependent stabilization trend, where short simulations capture initial flexibility, intermediate simulations reflect conformational adaptation, and longer simulations (25 ns) achieve dynamic convergence. When interpreted alongside RMSD data, these findings confirm that AdeB preserves a stable global fold while maintaining localized flexibility essential for efflux function. This validates the use of extended MD simulations for reliable structural and mechanistic interpretation and supports the robustness of downstream docking and inhibitor interaction analysis.

3.8.3. Radius of Gyration (Rg) Analysis of the AdeB Efflux Pump

The radius of gyration (Rg) analysis was performed to evaluate the overall structural compactness and folding stability of the AdeB efflux pump during molecular dynamics simulations at different time scales (1 ns, 10 ns and 25 ns). During the 1-ns MD simulation, the Rg values fluctuated within a narrow and stable range of approximately 2.42-2.56 nm (Figure 6C-i), indicating that protein maintained a consistent global conformation without signs of unfolding or abnormal expansion. A minor transient increase around the midpoint of the simulation likely reflects natural breathing motions of the protein, followed by gradual stabilization toward the end of the trajectory. In the 10-ns MD simulation, the Rg profile (Figure 6C-ii) exhibited moderately higher fluctuations compared with the 1-ns run, reflecting enhanced conformational sampling as the protein explored a broader configurational space. Despite these fluctuations, no abrupt increases or destabilizing trends were observed, confirming preservation of the folded state and structural integrity. Notably, the 25-ns MD simulation demonstrated a clearer stabilization pattern (Figure 6C-iii), with Rg values progressively decreasing and converging around ~2.15-2.25 nm after the initial equilibration phase. This reduction indicates increased structural compactness and tighter packing of the protein over extended simulation time, confirming attainment of

Creative Commons Attribution-Non-Commercial 4.0 International License

Published by DAC Democratic Arabic Center
DAC Democratic Arabic Center GmbH, Berlin

a more equilibrated and energetically favourable conformation. Collectively, the comparative Rg analysis reveals a time-dependent refinement of AdeB structural compactness, where longer simulations (25 ns) provide a more stable and physiologically relevant representation of the protein architecture. The absence of sharp spikes or large-scale expansion across all simulations confirms that AdeB preserves its folded conformation, consistent with the rigid transmembrane core characteristic of RND efflux pumps. These findings support the robustness of the AdeB model and reinforce its suitability for reliable docking, dynamic interpretation and inhibitor interaction analysis.

3.8.4. Solvent –Accessible Surface Area (SASA) Analysis of AdeB Efflux Pump

The solvent accessible surface area (SASA) was analysed to evaluate solvent exposure and global structural compactness of the AdeB efflux pump across different molecular dynamics simulation times (1 ns, 10 ns and 25 ns), as shown in Figure 6D (i-iii), distinct time depended stabilization patterns were observed. During the 1-ns simulation (Figure 6D-i), SASA values initially fluctuated around ~195 nm^2 within the first ~100 ps, followed by a gradual decrease and stabilization near 182-185 nm^2. This behaviour confirms early surface rearrangements and initial compaction of solvent exposed regions without structural destabilization. On other hand, in the 10-ns simulation(Figure 6D-ii), SASA values exhibited broader fluctuations during the early phase, followed by partial stabilization around 175-180 nm^2. This indicates increased conformational sampling and progressive reorganization of surface exposed loops, reflecting intermediate equilibration of the protein structure. Notably, the 25-ns simulation (Figure 6D-iii) demonstrated a pronounced and sustained reduction in SASA values, stabilizing around 150-158 nm^2 for the majority of the trajectory. This marked decrease indicates enhanced structural compaction and reduced solvent exposure, consistent with attainment of a more equilibrated and energetically favourable conformation. Importantly, no abrupt spikes or irregular drops were observed any of the simulations, confirming the absence of unfolding events or expansion. Overall, the comparative SASA analysis highlights a clear time dependent refinement of protein packing, with the extended 25-ns simulation providing the most stable and physiologically relevant conformational state of the AdeB efflux pump. This stabilized structure therefore represents a robust foundation for reliable docking interpretation and mechanistic inhibitor binding analysis.

Creative Commons Attribution-Non-Commercial 4.0 International License

Published by DAC Democratic Arabic Center
DAC Democratic Arabic Center GmbH, Berlin

3.8.5. Hydrogen Bonding Profile of the AdeB Efflux Pump

Hydrogen bonding is a critical indicator of protein structure stability and intramolecular cohesion during molecular dynamics simulations. Hydrogen bonding plays a fundamental role in maintaining protein structural integrity and intramolecular stability during molecular dynamics simulations. The hydrogen bond analysis of AdeB across different simulation times (1-ns, 10-ns and 25-ns) revealed a consistently robust and well-maintained hydrogen bonding network (Figure 6E (i-iii)). During the 1-ns simulation, the number of hydrogen bonds fluctuated moderately between approximately 170-195 bonds, particularly during the early equilibration phase, reflecting initial structural relaxation in the solvent environment. Despite these early fluctuations, the hydrogen bond count remained relatively stable, indicating preserved structural cohesion. Extension of the simulation to 10 ns resulted in a higher average number of hydrogen bonds (~180-205 bonds), accompanied by increased fluctuation density. This behaviour reflects enhanced conformational sampling and dynamics rearrangement of side chains while maintaining overall protein stability. Notably, the 25-ns simulation exhibited a more refined and stabilized hydrogen bond profile, with values consistently cantered around ~180-205 bonds and reduced long-range fluctuations. This stabilization confirms the establishment of a mature intramolecular hydrogen bonding network, indicative of improved structural equilibration and long-term conformational robustness. Collectively, the time- dependent hydrogen bonding patterns strongly correlate with RMSD, RMSF, Rg, SASA analysis, overall confirming that extended MD simulation enhances the structural reliability and dynamic stability of the AdeB efflux pump. The sustained hydrogen bond network observed at 25 ns supports the suitability of this equilibrated structure for downstream molecular docking and inhibitor interaction study.

The integrated molecular dynamics parameters including RMSD, RMSF, radius of gyration Rg, solvent accessible surface area (SASA), and hydrogen bonding analysis – collectively confirm that the AdeB efflux pump maintains excellent structural stability, consistent compactness and physiologically relevant flexibility across extended simulation times of 1-ns, 10-ns, 25-ns. While the short-term simulation (1 ns) captured the initial equilibration behaviour of the protein, longer simulations (10 ns and 25 ns) provided deeper conformational sampling and revealed progressive stabilization of global and local structural features. Notably, the 25 ns trajectory exhibited reduced RMSD and RMSF fluctuations, enhanced compactness reflected by stabilized Rg

Creative Commons Attribution-Non-Commercial 4.0 International License

Published by DAC Democratic Arabic Center
DAC Democratic Arabic Center GmbH, Berlin

values, decreased solvent exposure indicated by SASA convergence, and well-established intramolecular hydrogen bonding network. The absence of disruptive structural deviations across all simulation lengths demonstrates that AdeB preserves its native fold and dynamic integrity under simulated physiological conditions. These finding validate the robustness and reliability of the predicted AdeB structural model and strongly support its suitability for downstream inhibitor binding evaluation, mechanistic interpretation, and structure- based drug discovery efforts targeting efflux-mediated multidrug resistance in *Acinetobacter baumannii* isolates. Furthermore, the improved equilibration observed in extended simulations provides a solid structural foundation for interpreting the molecular docking results and strengthens the subsequent discussion on the inhibitory potential of PaBn and Pyridopyrimidine.

4. Discussion

The detection of 47 clinical *Acinetobacter baumannii* isolates (13.3%) from 354 clinical samples is consistent with global epidemiological observations, where *A. baumannii* is increasingly recognized as a major cause of hospital –acquired infections [33]. Numerous studies have reported similar prevalence rates ranging between 10-20% among hospitalized adults, especially in patients with prolonged hospitalization, mechanical ventilation or prior antibiotic exposure [1]. The high recovery of isolates from sputum, blood and wound swabs aligns with the pathogen's well-established tropism for respiratory tract infections, bacteraemia and wound colonization. This distribution mirrors previous reports demonstrating that respiratory samples typically constitute the primary source of where *A. baumannii* isolates worldwide [34]. The concordance between phenotypic identification –using CHROM agar, biochemical profiling and Vitek2 GN and the final molecular confirmation strengthens the reliability of the diagnostic workflow used in this study. Prior literature has emphasized that integrating automated biochemical systems with molecular methods significantly improves diagnostic accuracy, reduces misidentification and is particularly valuable for distinguishing *A. baumannii* from closely related species within the A. *baumannii* complex [35]. Collectively, these findings confirm the clinical importance of *A. baumannii* among hospitalized patients in Najaf and highlight the necessity of accurate laboratory identification as a foundation for antimicrobial susceptibility testing, infection control and genomic level investigations.

Creative Commons Attribution-Non-Commercial 4.0 International License

Published by DAC Democratic Arabic Center
DAC Democratic Arabic Center GmbH, Berlin

The antibiotic susceptibility profile in the present study demonstrates an alarming pattern of extensive drug resistance among the *A. baumannii* isolates, with complete resistance to imipenem, gentamicin, and amikacin, and very high resistance to meropenem, cefepime and ceftazidime. This resistance trend is consistent with global reports indicating that *A. baumannii* has emerged as one of the challenging pathogens due to its remarkable ability to acquire and disseminate resistance determinants [1]. The detection of 91.5% carbapenem –resistant *A. baumannii* (CRAB) aligns closely with findings from Middle Eastern and Asian clinical settings, where CRAB prevalence commonly exceeds 70-90% due to widespread carbapenem, prolonged stays, and increased environmental persistence of the organism [36]. Carbapenem resistance is primarily driven by OXA-type Carbapenemase, efflux pump overexpression, and horizontal gene transfer- mechanisms that collectively reduce β-lactam efficacy and complicate therapeutic management. Similarly, the high multidrug –resistance phenotype (MDR, 87.2%) is highly consistent with published surveillance data reporting MDR rates ranging from 70% to 95% in clinical *A. baumannii* isolates worldwide [40]. MDR *A. baumannii* strains are typically resistance to aminoglycosides, fluoroquinolones, β-lactams, and most cephalosporins, leaving clinicians with severely limited treatment options, often restricted to last-resort agents such as colistin or tigecycline [37,38]. The complete resistance to aminoglycosides (100%) and the high resistance rate to ciprofloxacin (82.9%) further support the hypothesis of resistance determinants via integrons, plasmids, and efflux pump over activation –particularly AdeABC –which are strongly associated with cross-resistance to multiple drug classes [39].

The molecular analysis revealed in this study an extensive distribution of resistance determinants among CRAB isolates, consistent with recent global surveillance reports. The universal detection of AdeB, *blaOXA-51, IMP, sul1* and *ESBL* genes indicates a highly resistant genomic background dominated by efflux pump overexpression, Carbapenemase activity and integron-mediated gene acquisition. Similar findings were reported in recent genomic based studies demonstrating that AdeABC efflux activation and OXA-type Carbapenemase constitute the major resistance drivers in *A. baumannii* worldwide [40]. The moderate prevalence of *blaOXA-23* (45%) aligns with regional studies showing variable dissemination but strong association with carbapenem resistance. The universal presence of *gyrB* among

Creative Commons Attribution-Non-Commercial 4.0 International License

Published by DAC Democratic Arabic Center
DAC Democratic Arabic Center GmbH, Berlin

CRAB isolates supports earlier evidence that mutations in topoisomerase genes contribute substantially to high –level fluoroquinolone resistance [41].

The sequencing and phylogenetic characterization of *AdeB* and *gyrB* in the present study revealed a highly conserved genetic architecture among CRAB isolates, consistent with global genomic surveillance reports. The strong conservation of AdeB supports its essential role within the AdeABC efflux system, which is known to be evolutionarily stable due to its critical contribution to multidrug resistance and bacterial fitness [41]. Similarly, the high identity observed (Figure.1) in *gyrB* aligns with previous findings indicating that topoisomerase genes undergo limited diversification, except for specific point mutations within the QRDR that drive fluoroquinolone resistance [42]. The formation of two phylogenetic clusters for both genes indicates natural micro- evolution and hospital –level clonal dissemination, a pattern frequently reported in endemic CRAB settings worldwide [43].

The structural characterization of the *AdeB* efflux pump in this study demonstrated a highly reliable and stereochemical sound 3D model, as supported by Ramachandran statistics and MolProbity geometry score (Figure 2E). The predominance of residues within favoured conformational regions (98.71%) and the absence of steric clashes or rotamer outliers collectively indicate excellent backbone geometry and validate the model's suitability for docking analysis. These findings are consistent with established benchmarks showing that high-quality membrane protein models typically exhibit >95% favoured residues and minimal angular outliers, particularly for RND –type efflux pumps such as AdeB [44]. Surface-rendered visualization further revealed well-defined pocket depressions and grooves (Figures 2A-D), corresponding to the functional substrate –binding and transport channels previously described for AdeB and other RND transporters [44].

The 2D structures of PaBn and Pyridopyrimidine derivative (Figures 2C-D) demonstrated functional groups essential for hydrogen bonding, aromatic stacking, and rotational flexibility, supporting their predicted capacity to fit into the binding chambers of *AdeB*. This aligns with prior structural analysis showing that efflux pump inhibitors (EPIs) require flexible hydrophobic –hydrophilic balance to gain access to the deep pockets within RND pumps [45]. Furthermore, the complete residue –level conservation observed in the multiple sequence alignment (Figure 2G) confirms high structural fidelity between the predicted *AdeB* model and the native reference sequence. The preservation of conserved motifs and transmembrane domains is consistent with

Creative Commons Attribution-Non-Commercial 4.0 International License

Published by DAC Democratic Arabic Center
DAC Democratic Arabic Center GmbH, Berlin

global genomic analysis demonstrating that *AdeB* is one of the most conserved resistance determinants in *A. baumannii* clinical isolates.

The docking analysis demonstrated that PaBn binds strongly to the AdeB efflux pump, with the C2 pocket showing the most favourable Vina binding energy (-9.1 kcal/mol), indicating a thermodynamically stable ligand –protein interaction. This energy level is consistent with previously reported efflux pump targeting inhibitors, where binding energies below -8.0 kcal are considered indicative of high-affinity interactions capable of competitively blocking substrate extrusion [6]. The observed network of stabilizing interactions-including hydrogen bonding (Ser83, Ser85, Thr88, Asp13), hydrophobic contacts (Phe8, Leu107, Phe117), and electrostatic pairing with acidic residues (Glu11, Glu12) aligns with established structural models describing AdeB substrate recognition and inhibitor engagement within the transmembrane pocket [46]. Furthermore, the binding of PaBn shown in the DSV generated 2D and 3D interaction maps (Figures 3A-D) is consistent with mechanisms reported for other small –molecule AdeB inhibitors, which typically insert into deep hydrophobic clefts while forming directional hydrogen bonds to anchor the ligand and reduce efflux pump mobility [47]. Comparable studies in multidrug –resistant *A. baumannii* have demonstrated that ligands stabilizing similar pocket environment can significantly impair efflux efficiency, thereby restoring antibiotic susceptibility.

The docking results demonstrated that Pyridopyrimidine binds favourable to the AdeB efflux pump, with pocket C1 showing the most thermodynamically stable interaction (-8.3 kcal/mol). The remarkable large pocket volume (3956 $Å^3$) and optimal geometric accommodation suggest that C1 represents a functionally relevant binding region capable of interfering with substrate transport. The identified interaction including hydrogen bonds with Thr6, Thr116, and Ser118, hydrophobic packing with Phe8, Leu114, Phe117, and electrostatic contacts involving Glu11 and Arg123- mirror previously reported interaction patterns of known AdeB inhibitors highlighting mechanistic plausibility of Pyri as an efflux blocker. These interaction features align with structural studies indicating that AdeB proximal binding pocket plays a key regulatory role in substrate recognition and antibiotic extrusion, and disruption of these residues can effectively reduce efflux efficiency [48]. Furthermore, the strong consistency between 2D/3D interaction maps and the predicted binding energy reinforces the stability of Pyri within the C1 pocket, a property also observed in recent inhibitor AdeB docking analysis involving pyridine based or heterocyclic scaffolds

Creative Commons Attribution-Non-Commercial 4.0 International License

Published by DAC Democratic Arabic Center
DAC Democratic Arabic Center GmbH, Berlin

[49]. The docking data confirm that Pyridopyrimidine has meaningful inhibitory potential against AdeB, supported by stable multi-type interactions, favourable binding energy and high pocket complementarity. These finding are consistent with contemporary computational drug-discovery reports demonstrating that compounds with similar heterocyclic features exhibit strong affinity for RND-type efflux pumps and may serve as promising leads for MDR *A. baumannii* therapy [50].

The comparative docking analysis between PaBn and Pyridopyrimidine inhibitor demonstrates that both molecules possess a strong capacity to interact with the AdeB efflux pump; however, PaBn exhibited a distinctly higher binding affinity (-9.1 kcal/mol) relative to Pyridopyrimidine (-8.3 kcal/mol). This affinity difference aligns with the well –established principle that deeper hydrogen-bond networks, extensive hydrophobic packing, and charged interactions enhance ligand stability with multidrug efflux transporters such as AdeABC. PaBn displayed a richer interaction profile, forming multiple hydrogen bonds and electrostatic contacts that tightly anchor the ligand into the C2 pocket-features consistent with high-affinity efflux pump inhibitors reported in recent structural studies [51]. Although Pyridopyrimidine also engaged key catalytic and transport-associated residues, its interaction network was comparatively fewer, confirming that while the ligand can occupy and stabilize the C1 pocket, its inhibitory potential may be moderate relative to PaBn.

Structural complementarity visualized through 2D/3D DSV mapping further supported this distinction: PaβN exhibited superior conformational fit and pocket coverage, a hallmark of effective AdeB inhibition [52]. Collectively, these finding confirm that both compounds represent promising AdeB efflux pump inhibitor candidates, but PaBn emerges as the more potent lead, supported by stronger binding energy, enhanced intermolecular interactions, and better spatial accommodation. These results agree with recent reports advocating the targeting of AdeB as a viable strategy to counteract resistance in *A. baumannii* [53].

Interestingly, the two inhibitors preferentially occupied different binding pockets within AdeB. PaβN exhibited optimal binding within the C2 pocket, whereas Pyridopyrimidine preferentially occupied the larger C1 cavity. This observation may suggest distinct inhibitory mechanisms. The stronger interaction of PaβN within the more confined C2 pocket could facilitate more effective interference with substrate translocation pathways, consistent with its lower binding energy and richer interaction network. In contrast, Pyridopyrimidine binding within the larger C1 cavity may

Creative Commons Attribution-Non-Commercial 4.0 International License

Published by DAC Democratic Arabic Center
DAC Democratic Arabic Center GmbH, Berlin

primarily influence substrate recognition or conformational transitions associated with efflux activity. Although these mechanistic interpretations remain speculative and require experimental validation, the findings suggest that multiple functional regions of AdeB may represent viable target for efflux pump inhibition.

Normal mode analysis (NMA) provided a mechanistic understanding of the intrinsic flexibility and global motions of the AdeB efflux pump, revealing dynamic properties that are essential for substrate translocation. The deformability profile (Figure 5A) showed limited peak amplitudes restricted mainly to surface-exposed loops, consistent with the behaviour of RND transporters whose periplasmic and transmembrane domains maintain rigid architectures to preserve functional integrity. The B-factor pattern derived from NMA (Figure 5B) further supported this observation, demonstrating predominantly low atomic mobility with slight increases in flexible peripheral segments an expected hallmark of transporter proteins capable of cyclic conformational changes during drug efflux [54]. The low eigenvalue obtained (9.29857e-06) indicates that AdeB can undergo collective motions with minimal energetic cost (Figure 5C), such low frequency motions are characteristic of large membrane –associated efflux pumps, which rely on coordinated domain transitions to open and close their substrate pathways [55].

Molecular dynamics (MD) simulation were employed to evaluate the time-depended conformational stability of the AdeB efflux pump. Short simulations (1 ns) mainly captured early solvent relaxation and local structural rearrangements, whereas extension to 10 ns and 25 ns enabled broader conformational sampling and proper equilibration of the protein system. Similar observations have been reported for membrane-associated transport proteins, where short MD trajectories are often insufficient to reach stable dynamic states [56]. Time depended stabilization is characteristic of resistance nodulation division (RND) family efflux pump, which undergo collective domain motions and loop rearrangements associated with substrate recognition and transport. Extended MD simulations are therefore critical to accurately capture these motions and to provide a realistic framework for interpreting inhibitor-binding behaviour. The residue- wise RMSF analysis provides critical insight into the time dependent local dynamics of the AdeB efflux pump and reveals a clear progression toward dynamic equilibration with increasing simulation length. During the 1 ns simulation, elevated flexibility at the N-terminus and selected loop regions reflects intrinsic disorder and early relaxation behaviour commonly observed in membrane-

Creative Commons Attribution-Non-Commercial 4.0 International License

Published by DAC Democratic Arabic Center
DAC Democratic Arabic Center GmbH, Berlin

associated transport proteins, while the low RMSF values within the core domains confirm preservation of the structural scaffold [57]. A distribution of flexibility rigid core with mobile peripheral loops is a hallmark of functional efflux pumps and it is essential for substrate recognition and transport.

The radius of gyration (Rg) analysis provides a quantitative measure of global structural compactness and folding stability of the AdeB efflux pump across different simulation time scales. The stable Rg range observed during the 1 ns simulation indicates that AdeB rapidly achieves a folded and coherent global architecture, with only minor transient fluctuations attributable to intrinsic breathing motions rather than structural destabilization [58]. Stabilization is characteristic of membrane associated transporters with rigid transmembrane cores that resist large-scale unfolding in aqueous environments. The solvent-accessible surface area (SASA) analysis provides critical insight into time-dependent changes in solvent exposure and global structural compactness of the AdeB efflux pump. The progressive reduction and stabilization of SASA values observed across increasing simulation lengths indicate gradual surface reorganization and conformational refinement rather than structural instability. This long-term stabilization is consistent with tighter packing of surface loops and improved domain organization, features that are essential for maintaining functional integrity of RND efflux pumps during substrate transport [59].

Importantly, the dynamic behaviour observed during the MD simulations provides a useful framework for interpreting the molecular docking results obtained for PaBn and Pyridopyrimidine. The consistency between the observed stability metrics and favourable docking interactions supports the plausibility of the identified binding modes and suggests that the protein-ligand complex remained structurally stable throughout the simulation period. Together, these findings support the suitability of the AdeB model for structure-based inhibitor evaluation and reinforce the rationale for targeting efflux pump dynamics as a strategy to counteract multidrug resistance in *Acinetobacter baumannii* isolates. However, longer simulation times and experimental validation are required to further confirm the long-term stability and biological relevance of the predicted interactions.

The widespread distribution of carbapenem-resistant *A. baumannii* strains underscores the urgent need for robust surveillance and diagnostic protocols to control the dissemination of resistance determinants in clinical environments [60].

Creative Commons Attribution-Non-Commercial 4.0 International License

Published by DAC Democratic Arabic Center
DAC Democratic Arabic Center GmbH, Berlin

5. Conclusion

This study provides an integrated phenotypic, molecular, phylogenetic and in silico analysis of multidrug-resistant *Acinetobacter baumannii*, highlighting the widespread occurrence of resistance-associated determinants among CRAB isolates. the escalating therapeutic challenge posed by this pathogen in clinical settings. The universal detection of the AdeB efflux pump gene together with multiple Carbapenemase, ESBL, integron and fluoroquinolone resistance markers underscore the complex and multifactorial nature of antimicrobial resistance in this pathogen. Structural modelling and in silico analyses suggested that the AdeB efflux pump possesses suitable structural characteristics for structure-based inhibitor evaluation. Molecular docking indicated favourable interactions of both PaβN and Pyridopyrimidine with the AdeB efflux pump, with PaβN exhibiting slightly stronger predicted binding affinity. Molecular dynamics simulations further suggested a tendency toward structural stability of the modelled protein-ligand complexes during the simulation period. Overall, these findings suggest that AdeB may represent a promising target for future anti-resistance strategies against *A. baumannii* isolates. However, additional experimental validation, longer molecular dynamics simulations, and functional studies are required to confirm the biological relevance and therapeutic potential of the predicted interactions and to support rational design of novel efflux pump inhibitors aimed at restoring antibiotic susceptibility.

Acknowledgements

The author gratefully acknowledges my College, the College of Medicine, University of Kufa, particularly the Postgraduate Molecular Biology Laboratory, Department of Microbiology, for providing the laboratory facilities and research environment required to conduct this research. The author also gratefully acknowledges the University of Arkansas for Medical Sciences (UAMS), USA, for providing access to the WebGRO platform, which was used to perform GROMACS-based Molecular dynamics simulations in this study.

Author Contributions

Hawraa Natiq Kabroot AL-Fatlawy independently conceived and designed the study, performed all experimental procedures, conducted molecular and bioinformatics analysis, interpreted the data, and drafted and revised the manuscript. The author approved the final version of the manuscript

 Creative Commons Attribution-Non-Commercial 4.0 International License Published by DAC Democratic Arabic Center
DAC Democratic Arabic Center GmbH, Berlin

Conflict of Interest

The author declares that there are no competing financial or personal interests that could have influenced the work reported in this manuscript.

Ethics Statement

This study was conducted in accordance with the ethical principles of the Declaration of Helsinki and was approved by the Medical Ethics Committee, College of Medicine, University of Kufa, Iraq (Approval No. MEC-168, approved on 19 May 2025). All procedures involving clinical samples were performed in compliance with institutional guidelines and patient confidentiality was strictly maintained throughout the study. Written informed consent was obtained from all participants prior to sample collection.

Data Availability Statement

The partial *adeB* gene sequence generated in this study has been deposited in the DNA Data Bank of Japan (DDBJ) under accession number **LC918549 and is publicly available at :** https://www.ncbi.nlm.nih.gov/nuccore/LC918549 . All other data supporting the findings of this study are available within the article.

Funding

The author received no financial support related to the conduct of the research, preparation of the manuscript, or publication of this article.

References

[1] Wong, D., Nielsen, T. B., Bonomo, R. A., Pantapalangkoor, P., Luna, B., & Spellberg, B. (2017). Clinical and Pathophysiological Overview of Acinetobacter Infections: a Century of Challenges. *Clinical microbiology reviews*, *30*(1), 409–447. https://doi.org/10.1128/CMR.00058-16

[2] Kyriakidis, I., Vasileiou, E., Pana, Z. D., & Tragiannidis, A. (2021). Acinetobacter baumannii Antibiotic Resistance Mechanisms. *Pathogens*, *10*(3), 373. https://doi.org/10.3390/pathogens10030373

[3] WHO Bacterial Priority Pathogens List Advisory Group, Sati, H., Carrara, E., Savoldi, A., Hansen, P., Garlasco, J., Campagnaro, E., Boccia, S., Castillo-Polo, J. A., Magrini, E., Garcia-Vello, P., Wool, E., Gigante, V., Duffy, E., Cassini, A., Huttner, B., Pardo, P. R., Naghavi, M., Mirzayev, F., ... Tacconelli, E. (2025). The WHO Bacterial Priority Pathogens List 2024: a prioritisation study to guide research, development, and public health strategies against antimicrobial

 Creative Commons Attribution-Non-Commercial 4.0 International License Published by DAC Democratic Arabic Center
DAC Democratic Arabic Center GmbH, Berlin

resistance. The Lancet Infectious Diseases, 25(9), 1033-1043. https://doi.org/10.1016/S1473-3099(25)00118-5

[4] Coyne, S., Courvalin, P., & Périchon, B. (2011). Efflux-mediated antibiotic resistance in Acinetobacter spp. *Antimicrobial agents and chemotherapy*, *55*(3), 947–953. https://doi.org/10.1128/AAC.01388-10

[5] Magnet, S., Courvalin, P., & Lambert, T. (2001). Resistance-nodulation-cell division-type efflux pump involved in aminoglycoside resistance in Acinetobacter baumannii strain BM4454. *Antimicrobial agents and chemotherapy*, *45*(12), 3375–3380. https://doi.org/10.1128/AAC.45.12.3375-3380.2001

[6] Roy, S., Junghare, V., Dutta, S., Hazra, S., & Basu, S. (2022). Differential Binding of Carbapenems with the AdeABC Efflux Pump and Modulation of the Expression of AdeB Linked to Novel Mutations within Two-Component System AdeRS in Carbapenem-Resistant Acinetobacter baumannii. *mSystems*, *7*(4), e0021722. https://doi.org/10.1128/msystems.00217-22

[7] Opperman, T. J., & Nguyen, S. T. (2015). Recent advances toward a molecular mechanism of efflux pump inhibition. *Frontiers in microbiology*, *6*, 421. https://doi.org/10.3389/fmicb.2015.00421

[8] Lomovskaya, O., Warren, M. S., Lee, A., Galazzo, J., Fronko, R., Lee, M., Blais, J., Cho, D., Chamberland, S., Renau, T., Leger, R., Hecker, S., Watkins, W., Hoshino, K., Ishida, H., & Lee, V. J. (2001). Identification and characterization of inhibitors of multidrug resistance efflux pumps in Pseudomonas aeruginosa: novel agents for combination therapy. *Antimicrobial agents and chemotherapy*, *45*(1), 105–116. https://doi.org/10.1128/AAC.45.1.105-116.2001

[9] Zhang, L., Tian, X., Sun, L., Mi, K., Wang, R., Gong, F., & Huang, L. (2024). Bacterial Efflux Pump Inhibitors Reduce Antibiotic Resistance. *Pharmaceutics*, *16*(2), 170. https://doi.org/10.3390/pharmaceutics16020170

[10] Wilhelm, J., & Pos, K. M. (2024). Molecular insights into the determinants of substrate specificity and efflux inhibition of the RND efflux pumps AcrB and AdeB. *Microbiology (Reading, England)*, *170*(2), 001438. https://doi.org/10.1099/mic.0.001438

[11] Leus IV, Roberts SR, Trinh A, W. Yu E, Zgurskaya HI.2024.Nonadditive functional interactions between ligand-binding sites of the multidrug efflux pump

 Creative Commons Attribution-Non-Commercial 4.0 International License Published by DAC Democratic Arabic Center
DAC Democratic Arabic Center GmbH, Berlin

AdeB from Acinetobacter baumannii . J Bacteriol206:e00217-23. https://doi.org/10.1128/jb.00217-23

[12] Azab, H., Askar, A. M., El-Fadeal, N. M. A., Othman, A. A. A., Rayan, A. H., & Khattab, S. (2025). Detection of AdeAB, TetA, and TetB efflux pump genes in clinical isolates of tetracycline-resistant Acinetobacter baumannii from patients of Suez Canal University Hospitals. *BMC microbiology*, *25*(1), 63. https://doi.org/10.1186/s12866-024-03735-1

[13] Clinical and Laboratory Standards Institute. (2025). *Performance standards for antimicrobial susceptibility testing* (35th ed., CLSI Supplement M100). Clinical and Laboratory Standards Institute.

[14] Magiorakos, A. P., Srinivasan, A., Carey, R. B., Carmeli, Y., Falagas, M. E., Giske, C. G., Harbarth, S., Hindler, J. F., Kahlmeter, G., Olsson-Liljequist, B., Paterson, D. L., Rice, L. B., Stelling, J., Struelens, M. J., Vatopoulos, A., Weber, J. T., & Monnet, D. L. (2012). Multidrug-resistant, extensively drug-resistant and pandrug-resistant bacteria: an international expert proposal for interim standard definitions for acquired resistance. *Clinical microbiology and infection : the official publication of the European Society of Clinical Microbiology and Infectious Diseases*, *18*(3), 268–281. https://doi.org/10.1111/j.1469-0691.2011.03570.x

[15] Al-Khafaji, A. M., & Al-Fatlawy, H. (2025). Molecular Genotyping of gyrA, blaOXA-51, and blaOXA-23 Genes in Multidrug-Resistant Acinetobacter baumannii Isolated from Childhood Asthma Patients in Iraq. Egyptian Journal of Medical Microbiology, 34(4), 483-489. doi: 10.21608/ejmm.2025.386369.1658. https://ejmm.journals.ekb.eg/article_433501.html

[16] Al-Khafaji, A. M. K. . ., & AL-Fatlawy, H. N. K. . (2025). Prevalence of Resistance Genes Gyr B, Ade-B and NDM-1 in Acinetobacter baumannii from Asthmatic Children. *Kufa Medical Journal*, *21*(1). https://doi.org/10.36330/kmj.v21.i1.19690

[17] Verma, P., Tiwari, M., & Tiwari, V. (2018). In silico high-throughput virtual screening and molecular dynamics simulation study to identify inhibitor for AdeABC efflux pump of Acinetobacter baumannii. *Journal of biomolecular structure & dynamics*, *36*(5), 1182–1194. https://doi.org/10.1080/07391102.2017.1317025

[18] Słoczyńska, A., Wand, M. E., Bock, L. J., Tyski, S., & Laudy, A. E. (2023). Efflux-Related Carbapenem Resistance in *Acinetobacter baumannii* Is Associated with

 Creative Commons Attribution-Non-Commercial 4.0 International License Published by DAC Democratic Arabic Center
DAC Democratic Arabic Center GmbH, Berlin

Two-Component Regulatory Efflux Systems' Alteration and Insertion of ΔAbaR25-Type Island Fragment. International Journal of Molecular Sciences, 24(11), 9525. https://doi.org/10.3390/ijms24119525

[19] Ghamgosha, M., Shahrekizahedani, S., Kafilzadeh, F., Bameri, Z., Taheri, R. A., & Farnoosh, G. (2015). Metallo-beta-Lactamase VIM-1, SPM-1, and IMP-1 Genes Among Clinical Pseudomonas aeruginosa Species Isolated in Zahedan, Iran. *Jundishapur journal of microbiology*, *8*(4), e17489. https://doi.org/10.5812/jjm.8(4)2015.17489

[20] karami, F., Nazari, R., & Adeli, H. (2021). Detection of Genes Encoding Metallo-beta-lactamases in Carbapenem Resistant Acinetobacter baumannii. Journal of Kerman University of Medical Sciences, 28(6), 559-567. doi:10.22062/jkmu.2021.91827 . https://jkmu.kmu.ac.ir/article_91827_d9d7f9a22fdc132e68ce56ffdbf85ff8.pdf

[21] Emamgholitabar Malekshah, F., Gholami, M., Pahlavanian, M., & Goli, H. R. (2025). Investigating the prevalence of class 1, 2, and 3 integrons in carbapenem-resistant Acinetobacter baumannii isolated from burn wound infections. *Scientific Reports*, *15*(1), 31857. https://doi.org/10.1038/s41598-025-17577-y

[22] Kitiyodom, S., Khemtong, S., Wongtavatchai, J., & Chuanchuen, R. (2010). Characterization of antibiotic resistance in Vibrio spp. isolated from farmed marine shrimps (Penaeus monodon). *FEMS microbiology ecology*, *72*(2), 219–227. https://doi.org/10.1111/j.1574-6941.2010.00846.x

[23] Chuanchuen, R., & Padungtod, P. (2009). Antimicrobial resistance genes in Salmonella enterica isolates from poultry and swine in Thailand. *The Journal of veterinary medical science*, *71*(10), 1349–1355. https://doi.org/10.1292/jvms.001349

[24] Smiline, A., Vijayashree, J., & Paramasivam, A. (2018). Molecular characterization of plasmid-encoded *blaTEM, blaSHV* and *blaCTX-M* among extended spectrum *β*-lactamases [ESBLs] producing *Acinetobacter baumannii*. *British Journal of Biomedical Science*, *75*(4), 200–202. https://doi.org/10.1080/09674845.2018.1492207

[25] Waterhouse, A. M., Studer, G., Robin, X., Bienert, S., Tauriello, G., & Schwede, T. (2024). The structure assessment web server: for proteins, complexes and more. *Nucleic acids research*, *52*(W1), W318–W323. https://doi.org/10.1093/nar/gkae270

 Creative Commons Attribution-Non-Commercial 4.0 International License Published by DAC Democratic Arabic Center
DAC Democratic Arabic Center GmbH, Berlin

[26] Waterhouse, A., Bertoni, M., Bienert, S., Studer, G., Tauriello, G., Gumienny, R., Heer, F. T., de Beer, T. A. P., Rempfer, C., Bordoli, L., Lepore, R., & Schwede, T. (2018). SWISS-MODEL: homology modelling of protein structures and complexes. *Nucleic acids research*, *46*(W1), W296–W303. https://doi.org/10.1093/nar/gky427

[27] Liu, Y., Yang, X., Gan, J., Chen, S., Xiao, Z. X., & Cao, Y. (2022). CB-Dock2: improved protein-ligand blind docking by integrating cavity detection, docking and homologous template fitting. *Nucleic acids research*, *50*(W1), W159–W164. https://doi.org/10.1093/nar/gkac394

[28] López-Blanco, J. R., Aliaga, J. I., Quintana-Ortí, E. S., & Chacón, P. (2014). iMODS: internal coordinates normal mode analysis server. *Nucleic acids research*, *42*(Web Server issue), W271–W276. https://doi.org/10.1093/nar/gku339

[29] Lopéz-Blanco, J. R., Garzón, J. I., & Chacón, P. (2011). iMod: multipurpose normal mode analysis in internal coordinates. *Bioinformatics (Oxford, England)*, *27*(20), 2843–2850. https://doi.org/10.1093/bioinformatics/btr497

[30] Kovacs, J. A., Chacón, P., & Abagyan, R. (2004). Predictions of protein flexibility: first-order measures. *Proteins*, *56*(4), 661–668. https://doi.org/10.1002/prot.20151

[31] Abraham, M. J., Murtola, T., Schulz, R., Páll, S., Smith, J. C., Hess, B., & Lindahl, E. (2015). GROMACS: High performance molecular simulations through multi-level parallelism from laptops to supercomputers. *SoftwareX*, *1-2*, 19-25. https://doi.org/10.1016/j.softx.2015.06.001

[32] WebGRO for Macromolecular Simulations: https://webgro.uams.edu/ (Accessed: 2025-11-12).

[33] Hamidian, M., & Nigro, S. J. (2019). Emergence, molecular mechanisms and global spread of carbapenem-resistant *Acinetobacter baumannii*. *Microbial genomics*, *5*(10), e000306. https://doi.org/10.1099/mgen.0.000306

[34] Li, S., Jiang, G., Wang, S. *et al.* (2025).Emergence and global spread of a dominant multidrug-resistant clade within *Acinetobacter baumannii*. *Nat Commun* 16, 2787 (2025). https://doi.org/10.1038/s41467-025-58106-9

[35] Strateva TV, Sirakov I, Stoeva TJ, Stratev A, Peykov S.(2023). Phenotypic and Molecular Characteristics of Carbapenem-Resistant *Acinetobacter baumannii* Isolates from Bulgarian Intensive Care Unit Patients. Microorganisms. Mar 29;11(4):875. https://doi:10.3390/microorganisms11040875 . PMID: 37110301; PMCID: PMC10141887.

 Creative Commons Attribution-Non-Commercial 4.0 International License Published by DAC Democratic Arabic Center
DAC Democratic Arabic Center GmbH, Berlin

[36] Alibrahim A, Wani FA, Alruwaili OS, Altaymani S, Alharbi ZA, Alsubaiei S, Aldhuwayhi S, Alsaeed M, Alibrahim M. (2025).Prevalence and Resistance Profiles of *Acinetobacter baumannii* in ICU Patients in Saudi Arabia: A Systematic Review and Meta-Analysis. Antibiotics (Basel). 2025 Nov 7;14(11):1131. https://doi:10.3390/antibiotics14111131 . PMID: 41301626; PMCID: PMC12649208.

[37] Goncalves EK, Penwell WF, Fiester SE. (2025). Combating the Growing Threat of *Acinetobacter baumannii* Resistance. Antibiotics (Basel). 2025 Jul 9;14(7):694. https://doi:10.3390/antibiotics14070694 . PMID: 40723996; PMCID: PMC12291915.

[38] CLSI (2023). "Performance standards for antimicrobial susceptibility testing" in CLSI supplement M100. Ed. CLSI Antimicrobial Susceptibility Testing Subcommittee. 33rd ed (Wayne, PA: Clinical and Laboratory Standards Institute).

[39] Karampatakis, T., Tsergouli, K., & Behzadi, P. (2025). Carbapenem-Resistant *Acinetobacter baumannii:* Virulence Factors, Molecular Epidemiology, and Latest Updates in Treatment Options. Microorganisms, 13(9), 1983. https://doi.org/10.3390/microorganisms13091983

[40] Boutzoukas A, Doi Y.(2025). The global epidemiology of carbapenem-resistant *Acinetobacter baumannii*. JAC Antimicrob Resist. 2025 Jul 29;7(4):dlaf134. https://doi:10.1093/jacamr/dlaf134 . PMID: 40735512; PMCID: PMC12305305.

[41] Z. A. A.-K. . Kadham, "Detection of gyrA and parC Genes in Clinical Acinetobacter Baumannii Isolates", *Al-Mustansiriyah J. Sci.*, vol. 33, no. 4, pp. 57–62, Dec. 2022, https://doi:10.23851/mjs.v33i4.1188 .

[42] Manik, M. R. K., Mishu, I. D., Mahmud, Z., Muskan, M. N., & Emon, S. Z. (2025). Association of fluoroquinolone resistance with rare quinolone resistance-determining region (QRDR) mutations and protein-quinolone binding affinity (PQBA) in multidrug-resistant Escherichia coli isolated from patients with urinary tract infection. *Journal of Infection and Public Health*, *18*(6), 102766. https://doi.org/10.1016/j.jiph.2025.102766

[43] Abu Sabah E, Tobin LA, Lebreton F, McGann PT, Hamidian M. (2025). Phylogenomics, evolution and origin of multidrug-resistant *Acinetobacter baumannii* ST15. Microb Genom. 2025 Jul;11(7):001450. https://doi:10.1099/mgen.0.001450 . PMID: 40673430; PMCID: PMC12284407.

Creative Commons Attribution-Non-Commercial 4.0 International License

Published by DAC Democratic Arabic Center
DAC Democratic Arabic Center GmbH, Berlin

[44] Wilhelm, J., Kobylka, J., Sjuts, H., Vargiu, A. V., Malloci, G., Reitz, J., Seybert, A., Frangakis, A. S., & Pos, K. M. (2021). Structural and functional analysis of the promiscuous AcrB and AdeB efflux pumps suggests different drug binding mechanisms. *Nature Communications*, *12*(1), 6919. https://doi.org/10.1038/s41467-021-27146-2

[45] Thu Nguyen, T. H., Nguyen, H. D., Le, M. H., Hien Nguyen, T. T., Nguyen, T. D., Nguyen, D. L., Nguyen, Q. H., Oanh Nguyen, T. K., Michalet, S., Dijoux-Franca, G., & Pham, H. N. (2023). Efflux Pump Inhibitors in Controlling Antibiotic Resistance: Outlook under a Heavy Metal Contamination Context. *Molecules*, *28*(7), 2912. https://doi.org/10.3390/molecules28072912

[46] Saikia, S., Gogoi, I., Puzari, M., Sharma, M., & Chetia, P. (2024). Identification of novel drug targets to counteract efflux pump mediated multidrug resistance in Acinetobacter baumannii. *Gene Reports*, *37*, 102013. https://doi.org/10.1016/j.genrep.2024.102013

[47] Sales Leão, P. V., Ferreira, S., Oliveira, A., Mesquita, S., Lima-Net, S., Chavéz Gutierrez, S. J., Sampaio Nogueira, C. E., Cruz-Martins, N., Rufino Arcanjo, D. D., Barreto, H. M., & Lima Ferreira, J. H. (2022). Riparin-B as a Potential Inhibitor of AdeABC Efflux System from Acinetobacter baumannii. *Evidence-Based Complementary and Alternative Medicine*, *2023*(1), 1780838. https://doi.org/10.1155/2023/1780838

[48] Zack, K. M., Sorenson, T., & Joshi, S. G. (2024). Types and Mechanisms of Efflux Pump Systems and the Potential of Efflux Pump Inhibitors in the Restoration of Antimicrobial Susceptibility, with a Special Reference to *Acinetobacter baumannii*. Pathogens, 13(3), 197. https://doi.org/10.3390/pathogens13030197

[49] Jamshidi, S., Sutton, J. M., & Rahman, K. M. (2017). Computational Study Reveals the Molecular Mechanism of the Interaction between the Efflux Inhibitor PAβN and the AdeB Transporter from Acinetobacter baumannii. ACS Omega, 2(6), 3002-3016. https://doi.org/10.1021/acsomega.7b00131

[50] Tuo, Y., Tang, Y., Yang, R., Zhao, X., Luo, M., Zhou, X., & Wang, Y. (2023). Virtual screening and biological activity evaluation of novel efflux pump inhibitors targeting AdeB. *International Journal of Biological Macromolecules*, *250*, 126109. https://doi.org/10.1016/j.ijbiomac.2023.126109

[51] Tariq, A., Ahmed, A., Khatoon, A., & Karim, A. (2025). Identification of drug targets in pan-drug resistant Acinetobacter baumannii via whole genome

 Creative Commons Attribution-Non-Commercial 4.0 International License Published by DAC Democratic Arabic Center
DAC Democratic Arabic Center GmbH, Berlin

sequencing and subtractive genomics. *Computers in Biology and Medicine*, *197*, 111058. https://doi.org/10.1016/j.compbiomed.2025.111058

[52] Lazarova, M., Eicher, T., Börnsen, C., Zeng, H., Athar, M., Okada, U., Yamashita, E., Spannaus, I. M., Borgosch, M., Cha, H., Vargiu, A. V., Murakami, S., Diederichs, K., Frangakis, A. S., & Pos, K. M. (2025). Conformational plasticity across phylogenetic clusters of RND multidrug efflux pumps and its impact on substrate specificity. *Nature Communications*. https://doi.org/10.1038/s41467-025-66751-3

[53] Dudas, B., Decleves, X., Cisternino, S., Perahia, D., & Miteva, M. (2022). ABCG2/BCRP transport mechanism revealed through kinetically excited targeted molecular dynamics simulations. *Computational and Structural Biotechnology Journal*, *20*, 4195. https://doi.org/10.1016/j.csbj.2022.07.035

[54] Ahmad, S., Shaker, B., Ahmad, F., Raza, S., & Azam, S. S. (2019). Moleculer dynamics simulaiton revealed reciever domain of *Acinetobacter baumannii* BfmR enzyme as the hot spot for future antibiotics designing. *Journal of Biomolecular Structure and Dynamics*, *37*(11), 2897–2912. https://doi.org/10.1080/07391102.2018.1498805

[55] AL-Fatlawy HNK.(2026). Molecular Docking Analysis of Coumarin and Indole Derivatives Targeting the MexB and GyrB in Multidrug-resistant *Pseudomonas aeruginosa* Clinical Isolates. *J Pure Appl Microbiol.* 2026;20(3):2399-2415. https://doi:10.22207/JPAM.20.3.33

[56] Liu, H., Xiang, S., Zhu, H., & Li, L. (2021). The Structural and Dynamical Properties of the Hydration of SNase Based on a Molecular Dynamics Simulation. *Molecules (Basel, Switzerland)*, *26*(17), 5403. https://doi.org/10.3390/molecules26175403

[57] Al-Fatlawy, H. N. K. (2026). Molecular Conservation Analysis and Structure-Based Evaluation of the GyrB ATPase Pocket as a Potential Target for SPR719 in Carbapenem-Resistant Klebsiella pneumoniae Clinical Isolates. Biomedical and Biotechnology Research Journal, 10(3), 290–302. https://doi.org/10.4103/bbrj.bbrj_56_26

[58] Stevens, J. A., Grünewald, F., Van Tilburg, P. A., König, M., Gilbert, B. R., Brier, T. A., Thornburg, Z. R., & Marrink, S. J. (2023). Molecular dynamics simulation of an entire cell. *Frontiers in Chemistry*, *11*, 1106495. https://doi.org/10.3389/fchem.2023.1106495

 Creative Commons Attribution-Non-Commercial 4.0 International License Published by DAC Democratic Arabic Center
DAC Democratic Arabic Center GmbH, Berlin

[59] Beleva, E., Diukendjieva, A., Pajeva, I., & Tsakovska, I. (2025). Identification of Compounds With Potential Dual Inhibitory Activity Against Drug Efflux Pumps in Resistant Cancer Cells and Bacteria: Protocol for a Systematic Review. *JMIR research protocols*, *14*, e66197. https://doi.org/10.2196/66197

[60] Asokan, S.; Banerjee, N.; Saleem, M.; Atiyah, H.M.; Pandey, R.K.; Abbas, R.K.; Yousif, S.I.A.; Radhamanalan, G.; Parashar, A.; Gowtham, B.; et al. Healthcare associated infections (HAI): Insights into epidemiology, microbiology, and diagnostics. Diagn. Microbiol. Infect. Dis. 2026, 115, 117376, https://doi.org/10.1016/j.diagmicrobio.2026.117376.

Supplementary Table S1. Distribution of Acinetobacter baumannii isolates according to clinical specimen source.

Clinical specimen	Number of isolates (n=47)	Percentage (%)
Sputum	38	80.9
Blood	3	6.4
Wound swab	6	12.7
Total	47	100

Supplementary Table S2. Comprehensive antimicrobial susceptibility profiles (Susceptible, Intermediate, and Resistant categories) of the 47 clinical Acinetobacter baumannii isolates.

No	Antibiotic agent	Antibiotic class = n		
		Susceptible-S N=%	Intermediate-I N=%	Resistant-R N=%
1	Imipenem	0%	0%	(47/47,100%)
2	Meropenem	0%	(4/47, 8.5%)	(43/47, 91.5%)
3	Gentamicin	0%	0%	(47/47,100%)
4	Amikacin	0%	0%	(47/47,100%)
5	Ciprofloxacin	0%	(8/47, 17.1%)	(39/47, 82.9%)
6	Ceftazidime	0%	(7/47, 14.9%)	(40/47,85.1%)
7	Cefepime	(3/47, 6.4%)	0%	(44/47,93.6%)
8	Piperacillin/tazobactam	(4/47, 8.5%)	(3/ 47, 6.4%)	(40/47, 85.1%).

Creative Commons Attribution-Non-Commercial 4.0 International License

Published by DAC Democratic Arabic Center
DAC Democratic Arabic Center GmbH, Berlin